

DOE/NASA/51040-32
NASA TM-82671

NASA-TM-82671
19820013838

Experimental Performance of the Regenerator for the Chrysler Upgraded Automotive Gas Turbine Engine

LIBRARY COPY
JAN 1982
LEWIS RESEARCH CENTER
KSC-82-0013838

Jerry M. Winter and Ralph C. Nussle
National Aeronautics and Space Administration
Lewis Research Center

February 1982

FOR REFERENCE

NOT TO BE TAKEN FROM THIS ROOM

Prepared for
U.S. DEPARTMENT OF ENERGY
Conservation and Renewable Energy
Office of Vehicle and Engine R&D

DOE/NASA/51040-32
NASA TM-82671

Experimental Performance of the Regenerator for the Chrysler Upgraded Automotive Gas Turbine Engine

Jerry M. Winter and Ralph C. Nussle
National Aeronautics and Space Administration
Lewis Research Center
Cleveland, Ohio 44135

February 1982

Work performed for
U.S. DEPARTMENT OF ENERGY
Conservation and Renewable Energy
Office of Vehicle and Engine R&D
Washington, D.C. 20545
Under Interagency Agreement DE-AI01-77CS51040

NOTICE

This report was prepared to document work sponsored by the United States Government. Neither the United States nor its agent, the United States Department of Energy, nor any Federal employees, nor any of their contractors, subcontractors or their employees, makes any warranty, express or implied, or assumes any legal liability or responsibility for the accuracy, completeness, or usefulness of any information, apparatus, product or process disclosed, or represents that its use would not infringe privately owned rights.

Summary

An experimental investigation was conducted to characterize the performance of the regenerator system of the Chrysler upgraded automotive gas turbine engine. A test facility was designed and constructed to simulate engine operating conditions for both sides of the regenerator. Detailed measurements of regenerator performance were made over a wide range of operating conditions. The regenerator temperature effectiveness for heating the cold fluid varied from 91 percent at operating conditions simulating 100 percent of engine speed, to 97 percent at operating conditions simulating 50 percent of engine speed. These values were 1 to 2 percent higher than the Chrysler design values and compared well with those measured during engine testing at the Lewis Research Center. Regenerator heat transfer effectiveness, however, was 2 to 4 percent lower than temperature effectiveness over the range of test conditions. A method was developed whereby leakage values could be used to correct heat transfer effectiveness values from the 90-percent Chrysler design value to 89 percent if the leakage was 5 percent. Leakage measurements made at ambient-temperature static conditions were in the 4 to 7 percent range; so there is experimental evidence for correcting the Chrysler design values downward. The results reported herein have not been corrected for leakage but nevertheless indicate a lower value of heat transfer effectiveness. Enthalpy effectiveness and an "enthalpy corrected method" also gave lower heat transfer effectiveness. The evidence gathered suggests that gas turbine system performance should be based on heat transfer effectiveness corrected for leakage rather than on temperature effectiveness.

The flow velocity uniformity leaving the regenerator within the engine housing was considered acceptable, given the compact arrangement of the Chrysler design and the insensitivity of regenerator effectiveness to flow distortion. A flow baffle incorporated into the high-pressure-side inlet cover of the engine housing significantly improved the velocity uniformity as well as the temperature uniformity on the high-pressure side of the regenerator. No significant improvement in regenerator temperature effectiveness was measured with the baffle.

Tests were also conducted with a regenerator housing designed to provide more uniform axial flow over the full area on both sides of the regenerator core. Although the flow uniformity in the supply ducting was not perfect, the blockage effect of the regenerator core served to produce

uniform velocities. Because the average flow velocity was lower with the axial-flow housing, the low-pressure-side flow uniformity was improved on an absolute basis but was not significantly improved on a percentage basis. However, the axial-flow housing did significantly improve the temperature uniformity on the high-pressure side, where the most significant flow changes were made. The regenerator temperature effectiveness values were the same with the axial-flow housing as with the original engine housing. The heat transfer effectiveness values were 4 to 6 percent lower than the temperature effectiveness values. Hot-flow leakage measurements indicated leakage rates in the 6 to 10 percent range for the axial-flow housing. The increased leakage could be responsible for the lower heat transfer effectiveness values as compared with the original engine housing.

Imposing a 50-percent (90° segment) flow blockage 2.8 cm (1 1/8 in.) upstream of the high-pressure side of the regenerator significantly affected the velocity uniformity on the high-pressure side. However, the temperature uniformity was not changed. The regenerator temperature effectiveness was also unchanged, and the heat transfer effectiveness was only 1 to 2 percent lower than without the flow blockage. The lower heat transfer effectiveness could also be explained by larger leakage rates during the 50-percent blockage testing.

Loss of housing insulation, seal leakage, and wear were problems experienced during the test program. Factors that were determined to control seal life included assembly clearances, insulation integrity, the finish of the sliding surfaces, and material selection. A graphite-reinforced polyimide D seal was developed as an approach to solving seal wear and breakage problems. Engine testing with the new seal is recommended to evaluate its performance.

Torque and leakage measurements helped to determine the seal condition both before and during testing. Reliable leakage measurements are required to enable correction of theoretical heat transfer effectiveness. A standard method for calculating heat transfer effectiveness is required if accurate comparisons are to be made between engine manufacturers as well as with theory.

Ambient-temperature flow velocity distribution measurements produced the same general flow patterns as were found in the hot-flow testing. Quantitative measurements of velocity uniformity did not always show the same trends when ambient-temperature measurements were compared with hot-flow measurements.

Core pressure drop values were generally somewhat higher than the design values. We were unable to determine whether the design values were for a thick-wall or thin-wall matrix. Our measurements of matrix wall thickness indicated a thick-wall value—0.012 cm (0.0046 in.). Core pressure drop results are more consistent with design values for 0.013-cm (0.050-in.) wall thickness—slightly higher pressure drops.

Introduction

The performance gains available from advanced automotive gas turbine engines would allow significant savings of automotive fuel if they are introduced in significant numbers into the automotive fleet. In addition, advanced pollution standards may be met more easily, and a multifuel capability allows better utilization of oil resources and possible substitution of other fuels as technology progresses. To capitalize on the inherent advantages of the gas turbine engine, however, an efficient method of recovering the heat from the turbine exhaust is required. The Chrysler upgraded engine uses a ceramic rotary regenerator to perform this function.

The Chrysler Corp. has been developing automotive gas turbine engines for several years, as documented in references 1 and 2. The engine development program, including this regenerator development was originally funded by the U.S. Environmental Protection Agency and then by the U.S. Department of Energy; it was managed in its latter stages by the NASA Lewis Research Center; and it is documented in reference 3. Initial testing of the complete engine (ref. 4) indicated that the horsepower was below the design goal and that the specific fuel consumption was above the design goal. A corrective development program was launched to understand the reasons for the deficiencies and to develop improved components so that engine performance goals would be met.

A general-purpose test facility was designed and constructed at Lewis to facilitate detailed measurements of regenerator performance parameters over a wide range of operating conditions with various design configurations. The facility supplied compressed, hot air to the high-pressure side of the regenerator to simulate engine compressor discharge. A separate supply system provided hot combustion products to the low-pressure side of the regenerator to simulate engine turbine discharge. Extensive instrumentation, together with automated data gathering and reduction, was incorporated to provide detailed insights into regenerator operating characteristics. The test facility was also designed for flexibility and quick turnaround so that a variety of regenerator housing configurations could be evaluated.

The test facility at Lewis was the only place where the regenerator system of the Chrysler upgraded automotive gas turbine engine was tested as a separate component at simulated engine conditions. The results of complete engine tests, reported in reference 5, provided some comparisons of regenerator performance results. However, the regenerator test facility was designed to provide a timely and more complete understanding of the effect of flow distribution and leakage on the heat transfer process in the regenerator. Both engine test time and instrumentation were necessarily limited, and it was difficult to separate the influence of individual variables or to change one variable at a time in engine testing. Therefore data from these tests were compared with the design performance goals for the engine (ref. 1) and with the performance of the regenerator measured in the engine (ref. 5) as well as used to screen and develop regenerator system modifications for possible incorporation in the Chrysler engine. Data from these tests could also be used in the analysis and design of advanced regenerator systems and to provide a better understanding of the influence of regenerator performance on gas turbine engine performance.

The scope of the effort reported herein included determining the effect of flow distribution on the heat transfer and pressure drop of the regenerator. A comparison of flow distribution at ambient temperature with flow distribution at engine operating temperatures was included. The influence of a regenerator cover baffle designed to provide a more uniform flow distribution to the high-pressure side of the regenerator was evaluated. The effect on performance of a housing designed to provide more uniform, completely axial flow to both sides of the regenerator was also investigated. A 50-percent flow blockage (90° segment) was applied to the high-pressure inlet, and the results were compared with those of the unblocked case as well as with those of the engine housing case. A correlation of seal wear and leakage rate with installation clearances and regenerator drive torque is included for each configuration. Recommendations are made to assist in the development of future regenerative heat exchanger systems for automotive gas turbine engines.

Apparatus and Procedure

Test Facility

The experimental regenerator test facility was located in the Special Projects Laboratory at the Lewis Research Center. A schematic of the facility is shown in figure 1(a) and a photograph in figure 1(b). Two separate flow systems were used to supply the regenerator. The Center's central compressed-air system provided air to

both systems. An electric heater was located in the high-pressure-side inlet to raise the air temperature to simulate the engine's compressor discharge temperature. A backpressure control valve located in the high-pressure-side discharge line was used to control pressure at the engine design conditions. The low-pressure-side inlet incorporated a combustor, burning A-1 jet fuel, to provide the high-temperature combustion products needed to simulate the engine's turbine discharge conditions. The combustion products exited the regenerator cover, as in the engine, and were discharged to the atmosphere.

Regenerator Test Package

The regenerator core was a lithium aluminum silicate (LAS) ceramic disk shown in figure 2. The disk was 53 cm (21 in.) in diameter and 8.3 cm (3¼ in.) thick. The insert in figure 2 shows an enlarged view of the ceramic matrix structure. The triangular-shaped matrix passage geometry had a specified wall thickness of 0.009 cm (0.0035 in.) Elastomeric mounting pads bonded the ring drive gear to the outer diameter of the regenerator core. Figure 3 shows the complete core with its elastomeric-mounted ring drive gear ready to be installed in the regenerator housing. The housing for the Chrysler upgraded engine is shown in figure 4. High-pressure air from a single 15-cm- (6-in.-) diameter pipe visible at the right in figure 3 entered the two kidney-shaped entrances to the cover. The high-pressure-side outlet included the burner housing and the turbine inlet vortex manifold to conform to the actual engine configuration. To approximate the flow conditions at the exit of the power turbine, the combustion products entered the low-pressure side of the regenerator housing through a 15-cm- (6-in.-) diameter pipe installed in the usual location of the power-turbine shaft (noted in fig. 4). The combustion products from this pipe impacted a flat plate and exited radially through annular gaps at approximately the same location as the engine power-turbine exit diffuser. No attempt was made to induce swirl or to otherwise simulate the power-turbine exit flow directions.

Figure 5 shows the regenerator cover for the engine housing. Figure 6 shows the regenerator cover with a baffle installed to provide a more uniform flow distribution to the regenerator core. Figure 7 illustrates the modified flow passages with the baffle installed. The axial-flow housing designed to supply a more uniform flow distribution to both sides of the regenerator is illustrated in figure 8. The axial-flow housing with and without the regenerator core in place is shown in figure 9. The Chrysler regenerator seals were used with both the axial-flow housing and the original engine housing. The regenerator ring gear was coupled by a pinion gear, a torque and speed transducer, and a gearbox to a variable-speed electric motor. The resultant gear ratio between

motor and regenerator was 45, providing enough power to vary core speed over the desired range of values (12 to 32 rpm).

Instrumentation

The engine housing had a grid of 15 total pressure probes and 15 radiation-shielded thermocouples at the high-pressure-side outlet of the core, arranged as illustrated in figure 4. Both temperature and total pressure probes were located 1.3 cm (½ in.) downstream from the ceramic regenerator core. Static pressure taps were installed on the wall and on probes in midstream of the flow area. The static pressure taps and probes were manifolded together to serve as a reference for the total pressure probes.

The low-pressure side of the engine housing regenerator cover had a grid of 15 total-to-static (pitot) probes and 15 radiation-shielded thermocouples arranged as illustrated in figure 5. They were also located 1.3 cm (½ in.) downstream of the regenerator core when the cover was installed. The low-pressure side of the regenerator cover with the baffle installed had no temperature instrumentation. For this test series the low-pressure-regenerator outlet temperature was not available; so comparison of heat transfer effectiveness could not be made. The high-pressure-side inlet temperature was measured by three thermocouples located in the kidney-shaped inlet ducts as identified on figure 3. The low-pressure-side inlet temperature was measured by three thermocouples spaced 120° apart in the low-pressure inlet pipe (fig. 4).

The high-pressure-side inlet pressure was measured through a static tap in the cover within 2.5 cm (1 in.) of the regenerator face—identified on figure 1(b). The low-pressure-side inlet pressure tap location is shown in figure 4. Pressure differentials across both sides of the regenerator were measured with ΔP transducers. A range of 6.9 kN/m² (1.0 psi) was used on the high-pressure side, and a range of 13.8 kN/m² (2.0 psi) was used on the low-pressure side.

For the axial-flow housing, 15 total-to-static (pitot) probes and 12 thermocouple probes were installed on each regenerator outlet, as shown in figure 9(b). The five thermocouple probes used to measure the high-pressure-side inlet air temperature are noted in figure 9(b). A wall static pressure tap to measure high-pressure-side inlet pressure is noted in figure 9(b) at the same plane as the thermocouples. A similar arrangement was used for low-pressure-side inlet pressure and temperature. All thermocouples were Chromel-Alumel type K with a calibration range of 0° to 1260° C (32° to 2300° F). Close-tolerance wire was used to minimize temperature error.

All the pressure lines from the 30 probes were connected to a differential pressure transducer by means

of a rapid scanning valve. This permitted one transducer to measure all the probes in consecutive order when steady-state test conditions were established. The pressure transducer used had a range of 0 to 0.4 kN/m² (0.058 psi) or 0 to 0.1 kN/m² (0.019 psi) depending on the test conditions being measured.

The airflow rates were measured by flat-plate orifices designed and installed to ASME specifications. Orifice locations are indicated in figure 1(a). Fuel flow was measured with a turbine flowmeter. All the data were recorded on a high-speed central data acquisition system; selected instrumentation was recorded on strip charts in the control room.

Operating Procedures

The assembly of the regenerator core, seals, and cover was initially performed by Chrysler personnel to their design specifications. Later, after procedures were established and knowledge of the hardware was acquired, NASA personnel performed assembly operations. To determine seal performance and to check out assembly procedures, seal leakage at an ambient-temperature, static condition was measured. The high-pressure exit duct was sealed so that pressure could be applied to the regenerator seals. A rotameter was used to measure airflow, which was assumed to be leakage through the seals into the low-pressure side of the regenerator. A value of leakage equal to about 5 percent of the engine design flow value was felt by Chrysler personnel to represent acceptable seal leakage for a cold static test.

The regenerator was brought to the desired test conditions (1) by setting flow rate and temperature on the high-pressure side, (2) by setting regenerator core speed, (3) by setting flow rate and temperature on the low-pressure side, and (4) by adjusting pressure on the high-pressure side. The first test condition was usually the 50 percent simulated gas generator speed. The test variables were allowed to stabilize and the data point was recorded. The data consisted of a strip-chart recording of the differential pressures for velocity determination and a high-speed digital recording of all the remaining instrumentation. Data were taken over the range of design conditions listed in table I, which represent engine design conditions from 50 to 100 percent of gas generator speed.

Results and Discussion

The results are presented in five groups:

- (1) Engine housing with original cover
- (2) Engine housing with a baffle in the cover
- (3) Axial-flow housing
- (4) Axial-flow housing with 50-percent (90°) blockage of the high-pressure inlet

(5) Axial-flow housing with increased regenerator temperature gradients

For each of the five groups the information is presented in the following order: Presented first are the velocity distributions with ambient air flowing through the regenerator and then the velocity distributions at engine pressures and temperatures. Temperature distribution data are presented next. Regenerator drive torque, correlation with seal wear, and leakage measurements are discussed next. This provides a perspective against which regenerator effectiveness is presented. Regenerator pressure drop measurements are included, with data shown for each of the housing configuration variations.

Chrysler Engine Housing with Original Cover

Velocity distribution. – The initial test series was run with ambient air flowing through both sides of the regenerator. The flow rates for each test were calculated to simulate specific engine operating conditions by the following relationship:

$$W_{\text{test}} = W_{\text{design}} \left(\frac{\sqrt{T_{\text{design}}/T_{\text{test}}}}{p_{\text{design}}/p_{\text{test}}} \right)$$

where

- W weight flow, kg/sec (lb/sec)
 T gas temperature, K (°R)
 p gas pressure, kN/m² (psia)

The actual test conditions and the results are listed at the top of table II. Flow rates were set to simulate 70 and 90 percent of gas generator speed. Also included were flow rates to simulate the regenerator core Reynolds number at the engine's 100-percent design point and the maximum flow capability of the test facility. Several data points were taken with the regenerator rotating. Because no difference in the measured pressures was found from the nonrotating case, results are reported for nonrotating cases, except for the maximum facility flow conditions.

Individual velocity calculations for each of the pressure probes were made by using the following relationship:

$$v = \sqrt{\frac{2g \Delta p}{12\rho}} = \sqrt{\frac{2g \Delta p RT}{p}}$$

where

- v gas velocity, m/sec (ft/sec)
 ρ gas density, kg/m³ (lb/in³)
 Δp total-to-static pressure differential, kN/m² (psi)
 T absolute temperature, K (°R)

- p absolute pressure, kN/m² (psia)
 g gravitational constant, 9.8 m/sec² (32.17 ft/sec²)
 R gas constant, m/K (ft/°R)

Figure 10 illustrates the individual velocities calculated and their locations. An average velocity was calculated for each data point and is listed in table II. Also listed is the standard deviation of the 15 discrete velocities for each side of the regenerator. The standard deviation as a percentage of the average velocity provides an objective measure of the velocity uniformity. The percentage values for ambient flow are shown in figure 11(a). The high-pressure side was significantly less uniform at the low flow rates. The same data for the hot-flow cases are plotted in figure 11(b). The low-pressure side was less uniform at high flow rates, but the high-pressure side was more uniform. There is not a direct comparison between the ambient-flow data and the hot-flow data.

Another method of describing the velocity uniformity is with velocity maps where equal velocities are plotted as contour lines. The contour lines labeled 1.0 represent the average velocity, and the other lines express ratios of the average velocity. Thus a 1.4 contour line would have a velocity 1.4 times the average velocity. Likewise, a 0.6 contour line would have a velocity 0.6 times the average velocity. It was assumed that the velocity at the wall was zero in constructing the maps. The velocity maps for ambient flow are given in figure 12. The velocity distribution on the high-pressure side was similar over the flow range, with a high-velocity area in the upper corner associated with the larger inlet duct to the regenerator cover. The uniformity improved at the highest flow rate, as noted previously in figure 11(a). The velocity distribution on the low-pressure side was more uniform but contained two areas of higher velocity at the maximum flow rate.

The velocity maps for the regenerator at engine operating temperatures are shown in figure 13. The distribution on the high-pressure side was similar to that measured for the ambient-flow case. The best match was the maximum ambient-flow case with the 80-percent hot-flow case. The low-pressure side exhibited better uniformity for the hot-flow cases, with somewhat similar patterns between ambient and hot flow. Because these velocity representations were of the flow leaving the regenerator, the flow straightening caused by the regenerator core and its pressure drop are included in these data.

Temperature distribution.—Table II lists the average temperatures measured for both sides of the regenerator over the range of test conditions. The outlet temperatures were measured 1.3 cm (½ in.) downstream of the regenerator face by radiation-shielded thermocouples. The standard deviation of the temperature measurements is also given in table II to provide an objective value for the temperature uniformity. Figure 14 gives the

individual temperatures and their locations and shows how the average and the standard deviation were arrived at for a 100-percent-of-design-speed data point. Figure 15 shows the standard deviation of the measured temperatures expressed as a percentage over the range of test conditions. The percentage spread decreased as flow increased for the low-pressure side; the reverse was true for the high-pressure side. However, the absolute magnitudes of the temperature spreads were about the same ($\pm 31^\circ\text{C}$, $\pm 55^\circ\text{F}$) at the full flow conditions. A map of temperature isotherms for both sides of the regenerator is given in figure 16. The temperatures were highest near the top of the regenerator, where the hot gases had been cooled the least and the air had been heated the most.

Drive torque, seal wear, and leakage.—The torque required to drive the regenerator served to measure the power and provided a diagnostic indicator of the regenerator seal condition. Initial torque measurements were made over a range of hot operating conditions and these fell within the band indicated as nominal in figure 17. After several hot test sequences totaling 4 hours of regenerator operation, a test sequence produced the high torque readings denoted as “failed seal” in figure 17. As flow and pressure levels increased, sounds of distress from the regenerator led to test termination. Inspection of the regenerator system following disassembly indicated severe wear of the regenerator seals, loss of housing insulation, and some erosion of the regenerator core surface. Gear wear was also pronounced, and eight of the 10 elastomeric bonds between the ring gear and the regenerator core were cracked. It was postulated that loss of the housing insulation upstream of the low-pressure-side seal ring caused the problem. The insulation particles entered the flow stream and were carried to the regenerator face, where they became wedged into the seal area by the rotation of the core. These particles could cause the seal wear, core erosion, and high torque readings observed during the test. The high-friction, high-torque condition then could have caused elastomeric failure, which allowed skipping of the pinion drive gear over the ring gear. The loss of the housing insulation could have led to all the observed conditions. Some patching of the insulation had been done in the course of earlier testing, and it is probable that the patching was not sufficient to maintain the integrity of the housing insulation’s erosion-resistant surface.

A new regenerator core, new seals, and new housing insulation were installed in the engine housing. During the initial hot-test sequence, torque readings were in the “nominal band” of figure 17. After about 1 hour of hot testing the regenerator cover was removed, and the new seal was discovered to be almost completely worn in several areas. There was no loss of housing insulation in

this case and no other damage. The roughness of the core surface in the seal area was thought to be the cause of the rapid seal wear. The core was returned to the manufacturer for checkout and surface refinishing. Upon completion of refinishing a surface roughness measurement indicated an average roughness of 12.7 to 17.8 μm (500 to 700 $\mu\text{in.}$) on the hot face, and 10.2 to 12.7 μm (400 to 500 $\mu\text{in.}$) on the cold face. This compares with an average roughness of 0.5 μm (20 $\mu\text{in.}$) for the smooth ceramic hub of the regenerator core.

The refinished core and a new seal were installed in the engine housing with three intermediate gaskets instead of the two gaskets used previously. The result was a clearance of 0.104 cm (0.041 in.) for the seal space as compared with 0.081 to 0.086 cm (0.032 to 0.034 in.) for the previous assemblies. A series of torque measurements during subsequent hot testing gave torque readings lower than any of the previous data, as indicated in figure 17. Inspection of the seal after 1 hour of hot-gas testing revealed no significant seal wear. The combination of increased clearance and reduced surface roughness resulted in lower torque readings and solved the rapid seal wear problem experienced during initial tests with this regenerator core.

To help determine the condition of the regenerator seals during this phase of testing, measurements of cold, static seal leakage were made. Instrumentation problems prevented hot dynamic leakage measurements during this phase of the program. For cold, static leakage the high-pressure exit was sealed so that the high-pressure side of the regenerator could be pressurized. Then with the low-pressure side open to the atmosphere, flow measured into the high-pressure side was assumed to be leakage across the seals. The regenerator core was not turning during these measurements. Cold, static leakage data were taken for two seal clearance values and are shown in figure 18. The data represented by the circles for the 0.086-cm (0.034-in.) clearance indicate about 6 percent leakage. After 1½ hours of hot testing, a repeat cold, static measurement indicated 9 percent leakage. Disassembly and inspection revealed the worn seal discussed previously. After the core was refinished, it was installed with a new seal and the clearance was increased to 0.104 cm (0.041 in.). The initial cold, static leak check in figure 18 indicated about 4 percent leakage. A check after 1 hour of rotation with ambient-temperature flow indicated 5 percent leakage. When the cover was removed, the seal seemed satisfactory; so the assembly was readied for hot testing. Another cold, static leakage measurement after reassembly indicated 6 to 7 percent leakage. After 1 hour of hot testing, another cold, static leakage measurement indicated 5 percent leakage (solid points in fig. 18). Although the seal was not worn after this test series, it was cracked and thus future tests required a new seal.

Seal wear and breakage problems led to an effort to develop an improved seal material for the wear face. A graphite-reinforced polyimide seal was fabricated at Lewis to meet the temperature, wear, and structural integrity criteria for the seal. (See fig. 19 for a photograph of the improved seal.) The experimental program reported herein was concluded before the improved seal became available. Therefore evaluation of the improvement was recommended for future engine tests.

Regenerator effectiveness.—The effectiveness of a regenerator is an indication of the amount of heat actually transferred as compared with the maximum possible heat transfer for a counterflow heat exchanger of infinite area. From reference 6 the heat transfer effectiveness is defined as

$$\epsilon = \frac{q}{q_{\max}} = \frac{C_h(t_{h,\text{in}} - t_{h,\text{out}})}{C_{\min}(t_{h,\text{in}} - t_{c,\text{in}})} = \frac{C_c(t_{c,\text{out}} - t_{c,\text{in}})}{C_{\min}(t_{h,\text{in}} - t_{c,\text{in}})}$$

where C_{\min} is the smaller of C_h and C_c

$$C_h = c_{p,h}W_h$$

$$C_c = c_{p,c}W_c$$

and

- $c_{p,h}$ specific heat of hot gas, J/kg °C (Btu/lb °F)
- $c_{p,c}$ specific heat of cold gas, J/kg °C (Btu/lb °F)
- W_h weight flow of hot gas, kg/sec (lb/sec)
- W_c weight flow of cold gas, kg/sec (lb/sec)
- $t_{h,\text{in}}$ hot-gas inlet temperature, °C (°F)
- $t_{h,\text{out}}$ hot-gas outlet temperature, °C (°F)
- $t_{c,\text{in}}$ cold-air inlet temperature, °C (°F)
- $t_{c,\text{out}}$ cold-air outlet temperature, °C (°F)

For the gas turbine flow conditions, C_{\min} is equal to C_c so that the heat transfer effectiveness becomes

$$\epsilon_{ht} = \frac{C_{p,h}W_h(t_{h,\text{in}} - t_{h,\text{out}})}{C_{p,c}W_c(t_{h,\text{in}} - t_{c,\text{in}})}$$

and the temperature effectiveness for heating cold fluid becomes

$$\epsilon_{tc} = \frac{C_{p,c}W_c(t_{c,\text{out}} - t_{c,\text{in}})}{C_{p,c}W_c(t_{h,\text{in}} - t_{c,\text{in}})}$$

In the second equation the specific heat and weight flow values cancel each other so that the temperature effectiveness for heating the cold fluid depends only on measured temperature values. Since this number is easier to calculate, it is the value most often reported in the experimental literature.

Both heat transfer effectiveness and temperature effectiveness will be reported herein, along with the numbers used for each calculation. The heat transfer effectiveness uses measured weight flows and specific heat values derived from NASA reference data.

Table II lists the experimental effectiveness values calculated for the regenerator with the original engine housing. Figure 20 compares the regenerator experimental values with the Chrysler design values of reference 4. The temperature effectiveness varies from 91 percent at 100 percent of engine design speed flow (0.61 kg/sec, 1.34 lb/sec) to 97 percent at 50 percent of design speed flow (0.20 kg/sec, 0.44 lb/sec). The heat transfer effectiveness varies from approximately 89 to 95 percent over the same flow range. One reason for the difference between the effectiveness values could be regenerator leakage. The Chrysler analysis of reference 4 indicates an expected leakage of 1.8 percent of the airflow supplied to the regenerator. The Chrysler analysis allocates 46 percent of the leakage to the low-pressure-side outlet of the regenerator, 46 percent to the low-pressure-side inlet to the regenerator, and 8 percent to the high-pressure-side outlet of the regenerator. If the Chrysler values are used to calculate regenerator heat transfer effectiveness at the 100-percent design point, the value is 90.0 percent with no leakage. Modifying the flow rates to reflect the 1.8 percent leakage value of Chrysler results in a heat transfer effectiveness of 89.6 percent. If the true leakage is 5 percent, as indicated by the cold, static leakage measurements, the corrected heat transfer effectiveness is 88.7 percent. The experimental value of heat transfer effectiveness averages 88.6 percent at 100-percent design flow. The temperature effectiveness for heating the cold fluid calculated from the design temperatures agrees with the no-leakage heat transfer effectiveness of 90 percent and is not changed by flow-rate changes. It is the authors' feeling that the heat transfer effectiveness values more accurately reflect the true regenerator performance. Besides the leakage correction explained previously, carryover losses are also present in the actual regenerator operation. Further discussion on leakage and correction calculations are given in later sections.

Figure 21 gives regenerator temperature effectiveness measured in actual engine testing as reported in reference 5. Performance was similar to that measured in the regenerator test facility, indicating a satisfactory simulation of the engine by the test facility.

Regenerator pressure drop. — The pressure drop across the regenerator core and the design pressure drops are shown in figure 22. The low-pressure-side pressure drops correlated well with the design values; the high-pressure-side pressure drops were higher than design. The results of reference 7 indicate that thin-wall regenerators have higher pressure drop than thick-wall regenerators—

mainly because of the difficulty of producing triangular passages with the thin-wall material. At the time of this work Chrysler specified 0.009-cm (0.0035-in.) wall thickness (thin wall). Earlier Chrysler specifications, however, listed the wall thickness as 0.013 cm (0.005 in.)—a thick wall. To determine the wall thickness of the tested regenerator, wall thicknesses were measured from the enlarged photograph of the core (fig. 2) and calculated from the known scale factors. The wall thickness derived by this method was 0.012 cm (0.0046 in.) with a variation of +0.004, -0.005 cm (+0.0017, -0.0019 in.). The measured values were closer to the thick-wall value, which, coupled with the good triangular shape, would produce pressure drops higher than the design values if the design pressure drops were for the thick-wall matrix.

Engine Housing with Baffle in Cover

Velocity distribution comparison. — The flow baffle in the high-pressure side of the engine housing was designed by Chrysler to provide a more uniform flow distribution across the regenerator face and to improve the heat transfer performance. The modified cover is shown in figure 6. Design details are shown in figure 7. The test data are summarized in table III. Velocity distribution measurements were confined to the high-pressure-air side of the regenerator since the baffle was designed to affect that side. A series of test measurements were made with ambient-temperature air. Duplicate measurements were made with the regenerator rotating and not rotating. Because no difference in velocities was measured, the data reported are those with a nonrotating regenerator. Figure 23 compares the standard deviation of the velocity measurements at ambient flow for the original cover and the modified (baffled) cover. The velocities with the baffled cover are significantly more uniform at low flow but about the same at high flow. Velocity maps illustrate the comparison over the flow range in figure 24. The low-velocity area at the bottom of the regenerator is seen to be improved over the test range. However, the high-velocity area at the top corner is accentuated by the baffle at the maximum ambient-flow rate.

Figure 25 illustrates no improvement in velocity uniformity for the baffled cover under hot-flow testing over the entire test range. Figure 26 shows velocity map comparisons for the hot tests. The maps look similar, with no significant redistribution of flow due to baffle installation. In this case the ambient-temperature flow results did predict the velocity uniformity trend of less uniform flow at higher flow rates.

Temperature distribution comparison. — The temperature uniformity comparisons were confined to the high-pressure-side outlet of the regenerator since the baffle was intended to influence flow on the high-

pressure side only. The cover with the baffle added was not instrumented to survey temperatures on the low-pressure-side outlet. The temperature uniformity on the high-pressure-side outlet for the original and modified covers is compared in figure 27. The uniformity is similar at the low flow rates, but the baffled cover gave improved temperature uniformity at the high flow rates.

The temperature distribution patterns for the high-pressure-side outlet with the original and modified covers are compared in figures 28 and 29. These isothermal maps were constructed from the data given by 14 thermocouples. The nature of the temperature distribution changed from a semicircular shape for the isotherms of the original cover to the approximately straight-across isotherms for the modified cover. Lowest temperatures for the modified cover were across the bottom of the regenerator; the lowest temperatures for the original cover were more toward the left center area. The modified cover achieved uniformity by decreasing the peak temperatures, particularly at the upper right of the high-pressure outlet.

Drive torque, seal wear, and leakage. – Regenerator torque values measured during testing with the modified cover are plotted in figure 30. Previous data are shown as bands associated with the clearance value used during assembly. By this time, it was concluded that the 0.102-cm (0.040-in.) clearance more nearly met seal wear and seal leakage criteria than did the 0.086-cm (0.034-in.) clearance used originally. The torque data indicate that the assembly with the modified cover performed as expected although at the high side of the band at the high-pressure condition.

Leakage measurements. – Leakage measurements were again made at ambient temperature with the high-pressure flow exit sealed so that any flow measured would be leakage through the regenerator seals. The regenerator was not rotating during these measurements. The data measured for this test series are plotted in figure 31. The increased clearance still allowed only a 5 percent leakage rate at the ambient condition. We assumed that the seals were in satisfactory condition on the basis of these measurements. An ambient-temperature test after the hot firing confirmed that there had been no change in the seal effectiveness as a result of the hot firing. The refinished regenerator installed with 0.102-cm (0.040-in.) assembly clearance and with the new seals was performing satisfactorily.

Regenerator effectiveness. – Table III lists the temperature effectiveness values calculated for the regenerator with the baffle added to the cover. Since this modified cover was not instrumented to determine the low-pressure-side outlet temperature $t_{h,out}$, the heat transfer effectiveness could not be calculated for this test sequence. Figure 32 illustrates the comparison between temperature effectiveness values with the original and

modified covers. The temperature effectiveness values with the modified cover were unchanged from those measured with the original cover. Although both velocity uniformity and temperature uniformity were improved by the baffle, there was no improvement in the regenerator temperature effectiveness.

Regenerator pressure drop. – The pressure drop across the regenerator core for the modified cover is shown in figure 31. All the measured pressure drops are higher than the design pressure drops. The pressure drop on the high-pressure side, where the baffle was installed, was essentially the same as that with the original cover. The pressure drop on the low-pressure side was higher than design over the whole test range, whereas with the original cover the pressure drop was higher than design only at the low flow rates (fig. 22).

Axial-Flow Housing

Velocity distribution. – The objective of the axial-flow housing design was to present the regenerator with an unrestricted uniform flow distribution on both sides. The hardware design is illustrated in figure 8. Basically, the space restriction of the engine housing was eliminated, and long tapered ducts were used to allow an axial approach to the regenerator. In addition, insulation projections and shelves were removed so that the entire face of the regenerator was open to the flow field.

A measure of the uniformity of flow velocity for the supply duct system is given in figure 34. These measurements were made without the regenerator in the system. The high-flow areas were associated with the elbows in the supply duct system. Various straighteners and flow distributors were applied to the duct system with minor improvement. The most effective flow straightener was the regenerator itself. The flow distribution of figure 35 illustrates the velocity uniformity with the regenerator in place at the same flow rate as used in figure 34. The velocities on the high-pressure side became more uniform as the flow rate increased. Figure 36 shows the velocity distribution at the maximum ambient-flow rate.

It was difficult to make accurate velocity measurements on the high-pressure side during the tests with the axial-flow housing. The signal-to-noise ratio was such that reliable values were difficult to derive from the data. Therefore most of the hot firings were able to produce data only for the low-pressure side of the regenerator. The most likely reason for the difference is that the axial-flow housing had no flow restrictions so that the increased flow areas decreased the absolute velocity level and thus decreased the signal-to-noise ratio. The relationship is illustrated in figure 37(a) for ambient-temperature airflow. Average velocities are seen to be only one-third as high as found with the engine housing.

Figure 37(b) illustrates the relationship for high-temperature airflow, which is even more pronounced. One data point was obtained when blockage upstream of the high-pressure inlet increased the average velocity to a measurable level. The comparison for the low-pressure side is given in figures 37(c) and (d). The exit velocities for the engine housing and the axial-flow housing were similar. The low-pressure side of the engine housing had no pronounced flow restrictions to increase velocity through the regenerator.

Flow velocity maps at hot operating conditions for the low-pressure side at 90 and 100 percent of simulated gas generator speed are shown in figure 38. The two high-velocity areas are similar to those found on the low-pressure side with ambient flow shown in figure 35. The statistical measure of velocity uniformity for both housings is compared in figure 39. The axial-flow housing was more uniform in terms of actual velocity (fig. 39(a)). However, because of the lower average velocities with the axial-flow housing, there was no clear advantage when the velocity uniformity was expressed as a percentage of the average velocity for the hot-flow tests (fig. 39(b)). In this case, the same conclusion could be drawn by comparing the ambient-temperature measurements for the two configurations (fig. 39(c)).

Temperature distribution. – The standard deviation of the measured temperature values is given in table IV. The standard deviation for the low-pressure side of the axial-flow housing is compared with the same data for the engine housing in figure 40. Improvement is noted only at the lowest flow rates tested. Figure 41 shows the comparison for the high-pressure side, where the axial-flow housing shows an improvement over most of the flow range. This is further illustrated in the isothermal maps of figure 42. Comparison with figure 16 for the engine housing reveals different-shaped isotherms on both sides as well as reduced temperature gradients. The axial-flow housing was successful in producing more uniform temperatures on the high-pressure side of the regenerator as compared with the engine housing, where inlet flow conditions were much more restricted.

Drive torque. – Considerable difficulty was experienced in sealing the axial-flow housing flanges against external leakage. Circular metallic O-ring seals were used initially without success. High-temperature gasket material was then used to solve the external leakage problem for the duration of one firing sequence. The clearance on the internal regenerator seals was initially set at a value of 0.109 cm (0.043 in.) to represent the modified values found to be satisfactory with the engine housing. However, to prevent external leakage, it was sometimes necessary to tighten down on the flanges more than was done with the engine housing. The result was to reduce seal clearance so that more torque was required to turn the regenerator. In addition, some

thermal distortion of the center cross arm of the housing was experienced. The distortion could also cause more friction on the regenerator, leading to high torque readings. The torque data are given in figure 43. The torques measured during each firing sequence fall into two groups: Group one compares well with the desirable range from the engine housing. Group two is near the values where seal failure was experienced with the engine housing. No seal failure or excessive wear was experienced during tests of the axial-flow housing. Cracking of the theta seal, which was caused both by thermal stress during hot firing and mechanical stress during assembly and disassembly, remained a problem throughout the entire test series. At any rate, torque values in the 114- to 171-N-m (1000- to 1500-in-lb) range were produced when seals were sufficiently clamped to keep leakage in the 6 to 10 percent range. Combining these torques with the regenerator speeds tested gave power values of 179 to 440 W (0.24 to 0.59 hp) for the above high torque range. The previous desirable range of torque values (57 to 114 N-m, 500 to 1000 in-lb) gave power values of 67 to 291 W (0.09 to 0.39 hp) for the same range of regenerator speeds.

Regenerator effectiveness. – The effectiveness values calculated for the Chrysler regenerator with the axial-flow housing are given in table IV and plotted in figure 44. The heat transfer effectiveness was about 5 percent lower than the temperature effectiveness. The temperature effectiveness was similar to the Chrysler design values, but at a flatter slope than the values measured previously with the original engine housing (fig. 20). The heat transfer effectiveness is similar to the engine housing values although somewhat lower, especially at the low flow rates. It may be concluded that the improvements in velocity and temperature uniformity produced by the axial-flow housing did not significantly improve the heat transfer performance of the regenerator. By making effectiveness values more uniform over the operating range, engine fuel consumption could be increased because of lower effectiveness at the low flow rates, where the engine must operate for a significant portion of its duty cycle.

Leakage measurement and influence on effectiveness. – During this test series it was possible to calculate leakage flow rates by measuring high-pressure airflows at the inlet and outlet of the test loop and then subtracting the two. The result is the total loss from the high-pressure side, including carryover and external leaks. We assumed that external leaks were minimized and that carryover was a function of the design that could not be controlled. However, the data plotted were the total losses from the high-pressure side, irrespective of leakage paths.

The leakage measurements for the test runs made with the axial-flow housing are plotted in figure 45. The

leakage started at 6 to 7 percent of rated airflow, near the previously measured cold, static data. Then it increased with increasing pressure difference across the seals until it reached 10 to 12 percent at the highest ΔP values simulating 100 percent of gas generator speed. It is not known if this leakage increase with increased pressure difference is typical of other regenerators or whether this characteristic is peculiar to the axial-flow housing. It could significantly change the values calculated for heat transfer effectiveness when corrections for leakage flows are taken into account. Most engine design calculations assume 2 to 5 percent leakage at the maximum-speed conditions.

There are many methods for calculating the influence of leakage on regenerator performance. Experimental results are discussed in reference 8. The Chrysler report of reference 4 gives leakage values and flow data for the regenerator studied here. A sketch of the Chrysler flow rates and leakage paths at 100-percent engine operating conditions is included as figure 46. Using the Chrysler temperature values to calculate temperature effectiveness yielded an effectiveness of 90 percent. As discussed previously, calculating the heat transfer effectiveness by using station 3 input (0.603 kg/sec, 1.3283 lb/sec) and adding fuel to derive the input gas flow, yielded an effectiveness of 90 percent for a no-leakage case. By using a leakage of 10 percent to modify the numerator and leaving the denominator at 0.603 kg/sec (1.3283 lb/sec), the corrected heat transfer effectiveness (upper) curve of figure 47 was derived. A different correction method would be to use the leakage flows to recalculate the weight flow actually passing through the core of the regenerator. By this method the heat transfer effectiveness would be calculated to increase to 95 percent at 10 percent leakage.

An alternative method described as an "enthalpy effectiveness" uses the leakage flow rates to calculate a heat flow rate at the inlet to the low-pressure side of the regenerator. This modified heat flow is used to calculate a modified temperature at this station by the relationship $Q = mc_p t$. Then the assumption is made that the regenerator is a constant-efficiency device so that a change in hot fluid inlet temperature will be balanced by a corresponding change in cold fluid outlet temperature. Making these calculations resulted in the data plotted as triangles in figure 47. The regenerator test facility data for uncorrected inlet flows to each side of the regenerator are plotted as solid points in figure 40. The leakage for the engine housing was assumed to be at the same percentage value hot as was measured cold. For the axial-flow housing, actual hot leakage measurements were used to plot the data, but the effectiveness values were still calculated by using measured input flows without leakage corrections. The test facility data fall between the two corrections where leakage is calculated to decrease

effectiveness. This declining effectiveness due to leakage was thought to be most likely for actual regenerator performance. The temperature effectiveness would not change significantly if the modified temperatures were entered into the calculation because both the low-temperature outlet (numerator) and the high-temperature inlet (denominator) would be assumed to change by the same ratio.

The wide range of values and methods for calculating heat transfer effectiveness illustrates the need for precise definition of the methods used when reporting these values. The authors recommend use of inlet flows to each side as a baseline. If leakage values and their distribution pathways are known, corrections may be applied, but the correction method should be described in detail. It would be helpful if the gas turbine industry could agree on a specific method for calculating regenerator heat transfer effectiveness.

Regenerator pressure drop.—Figure 48 shows the pressure drop across the regenerator in the axial-flow housing. The solid lines in figure 48 are the design specifications; the data points represent the extremes of the pressure drop data from table IV. The high-pressure-side pressure drop is close to the design specifications. The unrestricted flow and lower average velocities produced lower core pressure drop for the axial-flow housing than for the original engine housing.

The low-pressure-side pressure drop was still above the design specification as it had been for the engine housing with the baffle installed in the cover.

Axial-Flow Housing and 50-Percent (90° Percent Segment) Blockage of High-Pressure Inlet

Velocity distribution.—To measure the influence of severe flow blockage on regenerator effectiveness, a flat plate was installed at the entrance to the high-pressure side of the regenerator (fig. 49). The original installation was only 0.64 cm (¼ in.) upstream of the core, but thermal distortion of the flat plate during testing caused interference between the plate and the rotating regenerator. To avoid the interference problem, the plate was installed 2.86 cm (1⅛ in.) upstream of the regenerator. The velocity distribution produced is illustrated for ambient-flow conditions in figure 50. The flat plate reduced the velocities directly downstream to 60 percent and increased velocities over the remainder of the high-pressure side of the regenerator to 120 to 140 percent. The velocity map at 80 percent of simulated gas generator speed shows similar characteristics (fig. 51). Table V lists the actual velocity values and, although the standard deviation of the data was not significantly different on either side, the percentage variation was significantly greater on the high-pressure side because of the lower velocity average with the axial-flow housing (fig. 37(b)).

Temperature distribution. – The standard deviation of the temperature measurements on both sides of the regenerator (table V) was not significantly different from the standard deviation plotted in figures 40 and 41 for the axial-flow housing without flow blockage. Comparison of isothermal maps for 50 percent of simulated gas generator speed (fig. 52(a)), 80 percent of simulated gas generator speed (fig. 52(b)) and 100 percent of simulated gas generator speed (fig. 52(c)), illustrates the influence of increasing flow rate. The maps are similar to those of figure 42 for the axial-flow housing without flow blockage.

Drive torque. – The torques measured during this test series were close to the desirable range established with the engine housing and at 0.102-cm (0.040-in.) clearance (fig. 53). This indicates that assembly problems and/or thermal distortions suspected previously were minimized during this test series. The high torque readings shown in figure 43 have been eliminated.

Leakage measurements. – The leakage measurements made during the two hot-firing sequences are plotted in figure 54. Values from the initial firing sequence are similar to those of figure 45 for the axial-flow housing without blockage. The second firing sequence, however, indicates leakage of 10 percent or more over the entire test range. Since seal clearance (0.109 cm, 0.043 in.) and torque values were the same for the two firings, these increased leakage rates may be due to the design of the axial-flow housing and its associated thermal distortion. It may be concluded that less seal clearance, causing higher regenerator torque, may be required to prevent leakage of 10 percent magnitude for this housing design.

Regenerator effectiveness. – The data for regenerator effectiveness are listed in table V and plotted in figure 55. The temperature effectiveness values were seen to be about equal to those for the unblocked case (fig. 44). Heat transfer effectiveness, however, was 1 to 2 percent lower over the midrange for the cases with blockage and the same at either end of the flow range as the values of figure 44. A decrease in heat transfer effectiveness would be expected for the regenerator operation with the higher leakage values measured during this test series.

Regenerator pressure drop. – The pressure drop measurements for this test series are included in table V. The values are similar to those plotted in figure 48 with no blockage. The low-pressure-side ΔP values were again above the design values and slightly higher than the unblocked data at low flow rates.

Regenerator with increased temperature gradients. – A test sequence was run with the regenerator in the axial-flow housing to determine the temperature response of the regenerator when operated as a facility tool to heat air from 21° to 704° C (70° to 1300° F) for use in combustor testing. The regenerator normally operates with a 221° C (430° F) inlet air temperature; so the system would be

required to operate with a temperature difference 200° C (360° F) higher than normal.

As several test data points were being taken with ambient-temperature inlet air, the regenerator cracked and became completely separated from the drive mechanism. The failed regenerator is shown in figure 56. It is essentially similar to the failure of figure A.1.1 in reference 7.

The data taken during the firing sequence are listed in table VI. The test procedure was to change to progressively lower inlet temperatures and increased weight flow. The effect of decreasing inlet temperature was to apply a larger gradient across the regenerator, which created higher thermal stress. Neither torque nor leakage measurements were outside the range of previous data. The regenerator pressure drop, however, was significantly higher on both sides in the two readings made 10 minutes and 20 minutes prior to failure. The pressure drop measurements 32 minutes prior to failure were in the normal range. See figure 57 for these data. The only other change was to unbalance the flow, with lower flows on the high-pressure side than on the low-pressure side. No reason for the suddenly increased pressure drop was uncovered. The increased temperature gradients coupled with the unbalanced flow rates and increased pressure drop could all have contributed to the regenerator failure.

Concluding Remarks

On the basis of the data reported in NASA TM-81660, 1981 (Horvath, Ribble, Warren, and Wood) the regenerator test facility gave a satisfactory representation of regenerator operation in an actual engine. The ambient-flow velocity maps were a reasonable approximation of the hot-flow velocity maps. Calculated velocity uniformity as a percentage of the average did not always show the same results when ambient-flow measurements were compared with hot-flow measurements. The regenerator effectiveness was not sensitive to the kind of maldistribution of flow reported herein as demonstrated by the data for the engine housing with the baffle in the cover and with the axial-flow housing and one-half of the high-pressure inlet blocked. The difficulty of establishing completely uniform flow was illustrated by the axial-flow housing results without the regenerator core in place. The regenerator itself acted as a good flow distributor, and unless the particular engine system is insensitive to increased pressure drop, it is probably advisable to use the best design techniques in the allowable space without resorting to a large development effort to optimize flow distribution.

A more productive area for research would be in the development and demonstration of more effective seals

for the regenerator. The graphite-metal combination used herein was prone to cracking during assembly and disassembly operations. An effort by the Lewis Research Center to develop improved seals for the regenerator resulted in a seal constructed of a graphite-reinforced polyimide material. It is recommended that this seal be tested in an engine to demonstrate its improved performance and handling characteristics.

Leakage measurements indicated rates between 5 and 10 percent of rated airflow, rather than the 1.8 percent used in the design tables of SAE Paper 760279, 1976 (Ball, Gumaer, and Sebestyen). More difficulty was experienced in sealing the axial-flow housing than was anticipated, so that experience and development effort were required in this area. A trade-off between the torque required to turn the regenerator and the allowable leakage rate could be made. Our results indicated that torques in the range 59 to 171 N-m (500 to 1500 in-lb) also allow leakage in the range 5 to 12 percent.

The integrity of insulation upstream of the regenerator core is important in order to keep particles of insulation from lodging in the sliding seal and thus accelerating wear. Any other source of particles that might produce rapid wear must also be kept out of the upstream side of the regenerator. The surface finish of all regenerators, particularly in the rim seal area, must be checked before testing to ensure that accelerated seal wear will not be caused by the regenerator itself. Data reported herein indicated that surface roughness between (10.2 and 17.8 μm , 400 and 700 $\mu\text{in.}$) was satisfactory for the graphite seals used.

The uncertainty in the temperature measurements was calculated to be $\pm 1.9^\circ\text{C}$ ($\pm 3.5^\circ\text{F}$) at high-pressure-inlet temperatures (98° to 214°C , 209° to 417°F), $\pm 3.1^\circ\text{C}$ ($\pm 5.6^\circ\text{F}$) at high-pressure-outlet temperatures (706° to 718°C , 1302° to 1325°F), and $\pm 3.3^\circ\text{C}$ ($\pm 5.9^\circ\text{F}$) at low-pressure-inlet temperatures (767°C , 138°F). The uncertainty in the calculated temperature effectiveness was therefore ± 0.8 percent for one standard deviation. That compares with values from ± 0.2 percent to ± 0.8 percent for temperature effectiveness based on replicate measurements. The precision of the heat transfer effectiveness values, however, was between ± 1.0 and ± 1.8 percent for one standard deviation based on replicate measurements. The reason was the inclusion of weight flow (± 0.9 percent) and specific heat in the heat transfer effectiveness calculation.

An effort to eliminate uncertainties in the heat transfer effectiveness led us to make a calculation based on the enthalpy of the gases at each of the regenerator state points. A computer program developed at Lewis for use in turbojet engines was applied to the problem. A modification was necessary because the denominator of the effectiveness calculation contains gas temperature and air temperature both. It was necessary to convert gas

enthalpies to air enthalpies in order to be able to subtract Btu/lbm air from Btu/lbm air in the denominator. The resulting values for enthalpy effectiveness agreed with those calculated for heat transfer effectiveness. This was a further reason for preferring the heat transfer effectiveness values to represent effectiveness.

A method for calculating regenerator effectiveness should be agreed on for automotive gas turbine applications. Definitions of terms and exact relationships should be included in the standard method. Using temperature effectiveness, as defined herein, requires only three measured temperatures and provides more precise results. Using heat transfer effectiveness, however, requires three measured temperatures plus the specific heat and weight flow of each fluid. Precise definition of how specific heat and weight flow values are determined is therefore required. In this work we found significant differences between the two parameters used to describe heat transfer performance. It is felt that the heat transfer effectiveness is the better parameter for use in system design studies. Leakage values can be included in the calculation if desired, although the results reported herein do not include leakage corrections. In addition, heat transfer effectiveness agreed closely with enthalpy effectiveness for the axial-flow housing data, with and without blockage.

Comparing regenerator performance with design values is difficult unless the heat transfer and flow characteristics are known for the specific matrix under test. Pressure drops higher than design could result from matrix walls thinner than design. Effectiveness values less than design could result from matrix walls thicker than design. We measured matrix wall thickness of 0.012 cm (0.046 in.) as compared with a design value of 0.009 cm (0.0035 in.). Once the heat transfer parameters are known for a given wall thickness, a reliable inspection technique to determine wall thickness is required if meaningful comparisons between experimental and design performance are to be made.

References

1. Schmidt, F. W.; and Wagner, C. E.: Baseline Gas Turbine Development Program. QPR-10, Chrysler Corp., 1975. COO-2749-T10, 1975.
2. Ball, G. A.; Gumaer, J. I.; and Sebestyen, T. M.: The ERDA/Chrysler Upgraded Gas Turbine Engine—Objectives and Design. SAE Paper 760279, Feb. 1976.
3. Wagner, C. E. and Pampreen, R. C.: Upgraded Automotive Gas Turbine Engine Design and Development Program, Vol. 2. (DOE/NASA/2749-79/2-VOL-2, COO-2749-43; Chrysler Corp.; DOE Contract EY-76-C-02-2749.) NASA CR-159671, 1979.
4. Schmidt, F. W.; and Wagner, C. E.: Baseline Gas Turbine Development Program. QPR-18, Chrysler Corp., 1977. COO-2749-18, 1977.

5. Horvath, D.; et al.: Test Results of the Chrysler Upgraded Automotive Gas Turbine Engine—Initial Design. NASA TM-81660, 1981.
6. Kays, W. M.; and London, A. L.: Compact Heat Exchangers Second ed. McGraw-Hill Book Co., 1964.
7. Anderson, D. H.; et al.: Automotive Gas Turbine Ceramic Regenerator Design and Reliability Program. Annual Report for October 1, 1974—June 30, 1975. Ford Motor Co., 1975. COO-2630-1, 1975.
8. Matthews, C. C.: Measured Effects of Flow Leakage on the Performance of the GT-225 Automotive Gas Turbine Engine. SAE Paper 79-GT-3, Mar. 1979.

TABLE I. - RANGE OF DESIGN TEST CONDITIONS

(a) SI units

Test conditions	High-pressure-side flow, kg/sec	Low-pressure-side flow, kg/sec	High-pressure-side inlet temperature, °C	Low-pressure-side inlet temperature, °C	High-pressure-side inlet pressure, kN/m ²	Low-pressure-side inlet pressure, kN/m ²	Regenerator design speed, rpm
Cold-flow range	0.23 - 0.64	0.32 - 0.65	21	21	101.4	101.4	-----
50 Percent of gas generator speed	0.19	0.20	84	739	151.7	103.4	11.9
60 Percent of gas generator speed	.25	.25	103	741	180.6	104.1	15.5
70 Percent of gas generator speed	.31	.32	126	741	219.9	105.5	18.6
80 Percent of gas generator speed	.40	.41	153	742	271.7	106.9	20.3
90 Percent of gas generator speed	.49	.55	185	742	339.2	108.9	22.9
100 Percent of gas generator speed	.59	.60	221	743	417.8	111.7	22.9

(b) U.S. customary units

Test conditions	High-pressure-side flow, lb/sec	Low-pressure-side flow, lb/sec	High-pressure-side inlet temperature, °F	Low-pressure-side inlet temperature, °F	High-pressure-side inlet pressure, psia	Low-pressure-side inlet pressure, psia	Regenerator design speed, rpm
Cold-flow range	0.51 - 1.42	0.70 - 1.43	70	70	14.7	14.7	-----
50 Percent of gas generator speed	0.42	0.43	183	1362	22.0	15.0	11.9
60 Percent of gas generator speed	.55	.56	217	1365	26.2	15.1	15.5
70 Percent of gas generator speed	.69	.71	258	1365	31.9	15.3	18.56
80 Percent of gas generator speed	.875	.90	308	1367	39.4	15.5	20.34
90 Percent of gas generator speed	1.08	1.11	365	1368	49.2	15.8	22.85
100 Percent of gas generator speed	1.30	1.33	430	1369	60.6	16.2	22.85

TABLE II, - REGENERATOR PERFORMANCE

(a) SI

Simulated gas generator speed, percent	Regenerator speed, rpm	High-pressure-side airflow, kg/sec	Low-pressure-side gas flow, kg/sec	Average cold-air temperature		Average hot-gas temperature	
				Inlet, t_c , in $^{\circ}C$	Outlet, t_c , out $^{\circ}C \pm \sigma$	Inlet, t_h , in $^{\circ}C$	Outlet, t_h , out $^{\circ}C \pm \sigma$
Ambient-flow							
70	0	0, 272	0, 395	Ambient	Ambient	Ambient	Ambient
90	0	. 263	. 648				
$N_{Re} = 100$	0	. 318	. 318	↓	↓	↓	↓
Maximum facility flow	18, 4	. 608	. 513	↓	↓	↓	↓
Hot-flow test							
50	12, 0	0, 200	0, 207	98	737±8	758	173±41
60	16, 0	. 238	. 257	109	726±6	741	206±43
	16, 0	. 242	. 256	117	721±6	734	213±43
70	22, 5	. 324	. 321	132	698±16	729	199±28
	16, 4	. 333	. 327	144	704±16	736	212±26
	16, 0	. 324	. 322	138	722±19	749	260±37
80	25, 7	. 411	. 407	162	688±21	723	230±28
	18, 4	. 409	. 403	167	701±22	735	235±24
	18, 4	. 397	. 407	161	701±18	733	244±38
	18, 5	. 405	. 404	186	702±21	734	254±38
	18, 6	. 408	. 404	190	704±21	741	256±37
90	28, 9	. 515	. 513	184	702±26	740	261±29
	20, 7	. 493	. 517	198	706±24	742	276±25
	23, 0	. 511	. 521	209	691±23	726	287±36
100	32, 0	. 624	. 616	219	696±29	746	297±29
	32, 0	. 612	. 613	227	700±26	747	307±31
	23, 0	. 611	. 621	234	689±30	734	309±29
	23, 0	. 611	. 621	237	688±30	733	313±34

(b) U. S.

Simulated gas generator speed, percent	Regenerator speed, rpm	High-pressure-side airflow, lb/sec	Low-pressure-side gas flow, lb/sec	Average cold-air temperature		Average hot-gas temperature	
				Inlet, t_c , in $^{\circ}F$	Outlet, t_c , out $^{\circ}F \pm \sigma$	Inlet, t_h , in $^{\circ}F$	Outlet, t_h , out $^{\circ}F \pm \sigma$
Ambient-flow							
70	0	0, 60	0, 87	Ambient	Ambient	Ambient	Ambient
90	0	. 58	1, 43				
$N_{Re} = 100$	0	. 70	. 70	↓	↓	↓	↓
Maximum facility flow	18, 4	1, 34	1, 13	↓	↓	↓	↓
Hot-gas test							
50	12, 0	0, 433	0, 456	208	1359±14	1396	343±74
60	16, 0	. 524	. 566	229	1338±11	1366	402±78
	16, 0	. 533	. 565	242	1329±11	1354	415±78
70	22, 5	. 714	. 708	270	1289±28	1344	390±50
	16, 4	. 736	. 721	291	1300±28	1356	413±47
	16, 0	. 714	. 709	280	1332±35	1381	402±66
80	25, 7	. 905	. 899	323	1271±37	1333	446±50
	18, 4	. 902	. 889	333	1293±39	1355	455±43
	18, 4	. 875	. 898	322	1293±32	1352	471±68
	18, 5	. 892	. 891	366	1296±37	1353	489±69
	18, 6	. 900	. 890	374	1300±38	1365	492±67
90	28, 9	1, 136	1, 132	363	1295±46	1364	502±53
	20, 7	1, 086	1, 139	388	1302±44	1368	528±45
	23, 0	1, 126	1, 149	409	1275±42	1339	549±65
100	32, 0	1, 375	1, 357	427	1285±53	1375	567±52
	32, 0	1, 349	1, 351	440	1292±46	1377	585±55
	23, 0	1, 347	1, 370	454	1272±54	1354	589±53
	23, 0	1, 347	1, 370	459	1271±54	1351	595±61

- ENGINE HOUSING WITH ORIGINAL COVER

units

Low-pressure-side average gas velocity, m/sec ± σ	High-pressure-side average air velocity, m/sec ± σ	Temperature effectiveness for heating cold fluid, percent	Heat transfer effectiveness, percent	Torque, N-m	High-pressure-side pressure differential, kN/m ²	Low-pressure-side pressure differential, kN/m ²
---	--	---	--------------------------------------	-------------	---	--

test conditions

5.9±0.9	6.5±1.9	----	----	----	----	----
9.6±1.8	6.5±1.9	----	----	----	----	----
4.9±0.9	8.6±1.2	----	----	----	----	----
7.8±1.5	9.2±1.3	----	----	----	----	----

conditions

4.7±0.8	17.2±1.9	96.9	95.1	70	1.61	2.18
-----	-----	97.6	95.1	66	1.63	2.82
6.3±0.8	17.1±1.6	97.8	93.0	69	1.65	2.89
8.0±2.0	-----	94.9	90.7	102	1.83	3.65
7.7±1.8	22.0±1.8	94.7	90.0	91	1.78	3.21
-----	-----	95.5	91.5	72	1.55	3.09
10.9±2.3	-----	94.0	90.7	113	1.94	4.50
9.6±2.5	21.2±1.8	94.0	89.9	113	1.81	3.87
10.4±2.2	21.0±1.3	94.3	91.2	77	1.77	4.00
-----	-----	94.2	90.7	92	1.80	3.99
-----	-----	93.4	90.3	94	1.74	3.96
15.3±2.8	-----	93.1	88.7	154	2.17	5.81
12.7±3.1	20.9±2.8	93.3	92.5	143	1.93	5.04
13.7±2.6	27.7±3.1	93.1	90.0	107	1.75	5.21
36.3±7.1	-----	90.5	87.6	182	2.24	7.03
-----	-----	90.9	88.0	182	2.31	7.17
16.3±3.3	36.5±1.2	90.9	89.6	174	1.99	5.79
-----	-----	91.9	89.3	174	2.05	5.83

customary units

Low-pressure-side average gas velocity, ft/sec ± σ	High-pressure-side average air velocity, ft/sec ± σ	Temperature effectiveness for heating cold fluid, percent	Heat transfer effectiveness, percent	Torque, in-lb	High-pressure-side pressure differential, psi	Low-pressure-side pressure differential, psi
--	---	---	--------------------------------------	---------------	---	--

test conditions

19.5±3.1	21.3±6.1	----	----	----	----	----
31.4±6.0	21.3±6.1	----	----	----	----	----
16.0±2.8	28.1±3.9	----	----	----	----	----
25.7±4.9	30.3±4.4	----	----	----	----	----

conditions

15.3±2.6	56.4±6.2	96.9	95.1	612	0.233	0.316
-----	-----	97.6	95.1	581	.237	.409
20.7±2.7	56.0±5.1	97.8	93.0	608	.239	.419
26.3±6.7	-----	94.9	90.7	900	.266	.529
25.2±5.9	72.3±5.8	94.7	90.0	797	.258	.465
-----	-----	95.5	91.5	630	.225	.448
35.7±7.7	-----	94.0	90.7	990	.281	.652
31.4±8.2	69.7±5.9	94.0	89.9	990	.262	.561
34.2±7.2	69.0±4.2	94.3	91.2	675	.256	.580
-----	-----	94.2	90.7	805	.261	.579
-----	-----	93.4	90.3	825	.253	.574
50.1±9.2	-----	93.1	88.7	1350	.315	.843
41.6±10.2	68.7±5.1	93.3	92.5	1260	.280	.731
45.0±8.6	49.8±5.5	93.1	90.0	941	.254	.755
65.4±12.8	-----	90.5	87.6	1600	.325	1.02
-----	-----	90.9	88.0	1600	.335	1.04
53.5±10.7	65.7±4.1	90.9	89.6	1530	.288	.840
-----	-----	91.0	89.3	1530	.298	.846

TABLE III, - REGENERATOR PERFORMANCE -

(a) SI

Simulated gas generator speed, percent	Regenerator speed, rpm	High-pressure-side airflow, kg/sec	Low-pressure-side gas flow, kg/sec	Average cold-air temperature	
				Inlet, t_c, in °C	Outlet, t_c, out °C $\pm\sigma$
Ambient-flow					
50 70, 90 N _{Re} = 100	0	0.231	No flow	Ambient	Ambient
----- Maximum facility flow	↓	.272 .322 .490 .814	↓	↓	↓
Hot-flow test					
50	12	0.195	0.198	102	721±9
60	16	.234	.254	123	727±8
	16	.247	.258	117	710±8
70	18	.318	.318	153	704±12
80	20	.395	.399	186	688±16
90	23	.491	.510	223	697±17

(b) U. S.

Simulated gas generator speed, percent	Regenerator speed, rpm	High-pressure-side airflow, lb/sec	Low-pressure-side gas flow, lb/sec	Average cold-air temperature	
				Inlet, t_c, in °F	Outlet, t_c, out °F $\pm\sigma$
Ambient-flow					
50 70, 90 N _{Re} = 100	0	0.510	-----	Ambient	Ambient
----- Maximum facility flow	↓	.600 .710 1.080 1.340	----- ----- ----- -----	↓	↓
Hot-flow test					
50	12	0.430	0.436	215	1329±16
60	16	.537	.560	254	1341±14
	16	.544	.568	243	1311±14
70	18	.700	.702	308	1300±22
80	20	.870	.880	366	1270±29
90	23	1.083	1.124	433	1286±31

ENGINE HOUSING WITH BAFFLE ADDED TO COVER

units

Average hot-gas temperature		High-pressure-side average air velocity, m/sec $\pm \sigma$	Temperature effectiveness for heating cold fluid, percent	Torque, N-m	High-pressure-side pressure differential, kN/m ²	Low-pressure-side pressure differential, kN/m ²
Inlet, $t_{h, in}$, °C	Outlet, $t_{h, out}$, °C					

test conditions

----	---	7.9 \pm 0.8	----	----	-----	-----
----	---	7.6 \pm 1.0	----	----	-----	-----
----	---	8.7 \pm 1.1	----	----	-----	-----
----	---	9.0 \pm 1.6	----	----	-----	-----
----	---	9.7 \pm 1.8	----	----	-----	-----

conditions

745	138	-----	96.2	59	1.81	2.22
750	176	17.7 \pm 1.6	96.4	67	1.65	3.16
828	167	-----	96.7	57	1.77	3.21
732	195	21.4 \pm 2.2	95.3	81	1.78	3.98
721	229	17.4 \pm 2.0	93.9	94	2.02	5.59
729	275	15.5 \pm 1.9	93.6	122	2.07	8.00

customary units

Average hot-gas temperature		High-pressure-side average air velocity, ft/sec $\pm \sigma$	Temperature effectiveness for heating cold fluid, percent	Torque, in-lb	High-pressure-side pressure differential, psi	Low-pressure-side pressure differential, psi
Inlet, $t_{h, in}$, °F	Outlet, $t_{h, out}$, °F					

test conditions

----	---	26.1 \pm 2.7	----	----	-----	-----
----	---	25.0 \pm 3.3	----	----	-----	-----
----	---	28.7 \pm 3.7	----	----	-----	-----
----	---	29.6 \pm 5.2	----	----	-----	-----
----	---	31.9 \pm 5.8	----	----	-----	-----

conditions

1373	281	-----	96.2	517	0.262	0.322
1382	348	58.2 \pm 5.4	96.4	587	.240	.458
1347	333	-----	96.7	503	.257	.466
1349	382	70.2 \pm 7.3	95.3	711	.259	.577
1329	444	57.1 \pm 6.4	93.9	829	.293	.811
1344	527	50.9 \pm 6.3	93.6	1071	.30	1.16

TABLE IV. - REGENERATOR PERFORMANCE -

(a) SI

Simulated gas generator speed, percent	Regenerator speed, rpm	High-pressure-side airflow, kg/sec	Low-pressure-side gas flow, kg/sec	Average cold-air temperature		Average hot-gas temperature	
				Inlet, t_c, in $^{\circ}C$	Outlet, t_c, out $^{\circ}C \pm \sigma$	Inlet, t_h, in $^{\circ}C$	Outlet, t_h, out $^{\circ}C \pm \sigma$
Ambient-flow							
---	(a)	0.371	0.371	Ambient	Ambient	Ambient	Ambient
---	0	.371	.371	↓	↓	↓	↓
---	20	.517	.517				
---	0	.558	.558				
Maximum facility flow	0	.644	.594	↓	↓	↓	↓
Hot-flow test							
50	11.9	0.203	0.195	67	650±4	697	131±26
	12.0	.200	.187	69	701±9	747	145±32
60	15.8	.249	.249	123	667±4	693	191±24
	15.7	.258	.254	113	640±4	668	181±23
	15.6	.252	.254	94	683±6	715	182±30
	15.6	.264	.262	76	678±6	716	167±33
70	18.8	.318	.321	110	651±4	684	196±26
	18.7	.313	.318	128	662±3	691	210±25
	18.7	.329	.326	114	676±5	713	200±28
	18.7	.324	.334	134	708±6	748	231±33
	18.7	.327	.337	91	701±5	744	207±38
80	20.5	.395	.409	152	676±6	706	234±24
	21.6	.404	.398	133	647±4	683	223±27
	20.5	.419	.395	142	658±5	696	226±26
	20.7	.399	.396	121	646±4	683	209±26
	20.8	.396	.392	144	643±6	674	225±27
	20.5	.405	.413	141	669±4	703	234±27
	20.6	.406	.399	133	694±5	729	229±28
	20.4	.402	.405	133	663±6	707	224±29
	20.5	.406	.410	158	701±6	740	251±31
	20.5	.408	.410	130	688±5	728	224±30
90	23.2	.489	.492	182	680±6	711	267±23
	23.2	.491	.504	186	677±7	708	268±22
	23.3	.500	.498	193	657±8	688	273±26
	23.0	.498	.500	182	682±6	718	276±26
	23.0	.498	.500	193	679±6	710	286±26
	23.1	.503	.503	180	687±7	729	271±28
	23.3	.503	.512	198	696±6	736	296±31
	23.1	.513	.515	169	685±8	725	264±28
100	23.3	.586	.596	245	666±7	698	323±23
	23.3	.596	.603	244	662±8	692	321±22
	23.4	.598	.596	196	651±7	692	298±27
	23.5	.599	.598	203	649±7	689	305±27
	23.6	.606	.608	227	671±6	711	325±31
	23.3	.616	.619	206	683±9	725	302±29

^aWithout regenerator.

AXIAL-FLOW HOUSING

units

Low-pressure-side average gas velocity, m/sec $\pm \sigma$	High-pressure-side average air velocity, m/sec $\pm \sigma$	Temperature effectiveness for heating cold fluid, percent	Heat transfer effectiveness, percent	Leakage, percent of airflow	Torque, N-m	High-pressure-side pressure differential, kN/m ²	Low-pressure-side pressure differential, kN/m ²
--	---	---	--------------------------------------	-----------------------------	-------------	---	--

test conditions

5.5 \pm 5.2	3.5 \pm 3.9	----	----	----	----	----	----
6.1 \pm 1.2	4.3 \pm 1.3	----	----	----	----	----	----
7.7 \pm 1.0	-----	----	----	----	----	----	----
6.9 \pm 1.5	-----	----	----	----	----	0.669	1.158
7.3 \pm 1.6	3.2 \pm 0.5	----	----	----	----	.572	1.310

conditions

-----	-----	93.6	90.3	6.3	91	1.241	2.006
3.2 \pm 0.6	-----	93.3	88.8	7.3	48	1.303	2.214
5.5 \pm 1.2	-----	95.3	90.8	7.6	74	1.331	2.661
-----	-----	94.9	90.2	6.0	62	1.310	2.523
4.6 \pm 1.0	-----	94.8	89.9	5.9	113	1.462	2.820
4.6 \pm 0.9	-----	94.1	88.4	8.7	63	1.448	2.758
-----	-----	94.2	89.1	8.1	98	1.358	3.454
-----	-----	94.9	90.2	6.8	86	1.372	3.558
6.9 \pm 1.4	-----	93.6	88.3	7.4	130	1.482	3.530
6.9 \pm 1.3	-----	93.6	90.4	7.4	61	1.551	3.992
6.3 \pm 1.2	-----	93.4	88.4	8.9	85	1.551	3.868
-----	-----	94.4	91.7	6.9	108	1.351	4.357
9.0 \pm 1.7	-----	93.4	87.6	6.5	169	1.365	4.378
6.6 \pm 1.6	-----	93.3	84.9	9.9	156	1.358	4.378
8.0 \pm 1.6	-----	93.5	88.7	5.2	161	1.296	4.116
8.6 \pm 1.9	-----	94.1	88.7	7.2	162	1.331	4.075
8.6 \pm 2.1	-----	93.9	90.5	7.3	169	1.434	4.530
8.4 \pm 1.9	-----	94.2	87.5	10.6	151	1.482	4.647
8.9 \pm 1.9	-----	92.4	88.0	6.2	146	1.475	4.351
8.8 \pm 1.8	-----	93.2	88.5	7.1	79	1.544	4.675
8.5 \pm 1.7	-----	93.5	88.2	7.6	127	1.496	4.482
-----	-----	94.2	88.1	8.1	123	1.400	5.716
-----	-----	94.0	90.1	8.0	120	1.386	5.536
12.3 \pm 2.4	-----	93.7	88.5	8.1	188	1.413	5.440
11.8 \pm 2.0	-----	93.3	88.4	7.5	230	1.606	5.826
12.2 \pm 2.3	-----	94.0	87.7	7.8	166	1.496	5.978
11.9 \pm 2.5	-----	92.3	87.1	8.3	180	1.510	5.571
12.7 \pm 2.3	-----	92.5	87.1	6.9	124	1.538	6.088
11.8 \pm 2.1	-----	92.9	86.7	8.4	126	1.482	5.667
16.4 \pm 2.6	-----	93.0	87.8	6.4	129	1.427	6.812
-----	-----	93.5	87.4	9.5	151	1.386	6.895
-----	-----	91.6	87.4	9.6	168	1.372	7.102
-----	-----	91.9	84.2	9.2	179	1.407	7.033
15.6 \pm 2.8	-----	91.5	83.8	10.4	152	1.489	7.033
15.1 \pm 2.7	-----	91.9	86.0	8.1	149	1.496	6.819

TABLE IV. -

(b) U. S.

Simulated gas generator speed, percent	Regenerator speed, rpm	High-pressure-side airflow, lb/sec	Low-pressure-side gas flow, lb/sec	Average cold-air temperature		Average hot-gas temperature	
				Inlet, t_c , in ^a °F	Outlet, t_c , out ^a °F ± σ	Inlet, t_h , in ^a °F	Outlet, t_h , out ^a °F ± σ
Ambient-flow							
---	(a)	0.820	0.820	Ambient	Ambient	Ambient	Ambient
---	0	.820	.820	↓	↓	↓	↓
---	20	1.140	1.140				
----	0	1.230	1.230				
Maximum facility flow	0	1.420	1.310	↓	↓	↓	↓
Hot-flow test							
50	11.9	0.447	0.431	153	1213±8	1286	267±46
	12.0	.442	.412	157	1294±17	1376	293±58
60	15.8	.550	.548	253	1232±8	1279	375±44
	15.7	.568	.561	236	1184±8	1235	357±42
	15.6	.555	.560	202	1261±11	1319	359±54
	15.6	.582	.578	169	1253±11	1320	332±60
70	18.8	.702	.708	230	1203±8	1263	385±47
	18.7	.690	.702	262	1224±6	1275	410±45
	18.7	.725	.719	237	1248±9	1316	392±50
	18.7	.715	.737	273	1307±10	1378	448±60
	18.7	.721	.743	196	1293±9	1371	404±68
80	20.5	.871	.901	305	1248±10	1303	453±43
	21.6	.891	.878	272	1196±8	1261	434±48
	20.5	.923	.871	287	1217±9	1285	439±46
	20.7	.880	.874	250	1195±8	1261	409±47
	20.8	.874	.864	291	1190±11	1245	437±49
	20.5	.892	.910	285	1236±8	1298	454±49
	20.6	.896	.880	271	1282±9	1344	445±50
	20.4	.887	.892	271	1226±11	1304	436±52
	20.5	.894	.904	316	1293±10	1364	484±56
	20.5	.900	.904	266	1271±9	1342	436±54
90	23.2	1.077	1.084	360	1256±11	1311	513±41
	23.2	1.083	1.112	366	1251±13	1307	515±40
	23.3	1.103	1.098	380	1214±14	1270	524±47
	23.0	1.097	1.103	359	1259±11	1324	529±47
	23.0	1.099	1.103	379	1255±10	1310	546±46
	23.1	1.110	1.110	356	1269±13	1345	520±50
	23.3	1.109	1.128	389	1285±11	1357	565±55
	23.1	1.132	1.135	337	1265±14	1337	508±51
100	23.3	1.291	1.315	473	1231±13	1288	613±42
	23.3	1.313	1.329	471	1224±14	1277	610±39
	23.4	1.319	1.314	384	1203±12	1278	569±49
	23.5	1.320	1.318	397	1201±12	1272	581±49
	23.6	1.335	1.340	440	1239±10	1312	617±56
	23.3	1.358	1.364	406	1262±16	1337	575±52

^aWithout regenerator.

Concluded,

customary units

Low-pressure-side average gas velocity, ft/sec $\pm \sigma$	High-pressure-side average air velocity, ft/sec $\pm \sigma$	Temperature effectiveness for heating cold fluid, percent	Heat transfer effectiveness, percent	Leakage, percent of airflow	Torque, in-lb	High-pressure-side pressure differential, psi	Low-pressure-side pressure differential, psi
---	--	---	--------------------------------------	-----------------------------	---------------	---	--

test conditions

18, 2 \pm 17, 0	11, 4 \pm 12, 7	----	----	----	----	----	----
20, 0 \pm 4, 0	14, 1 \pm 4, 2	----	----	----	----	----	----
25, 3 \pm 3, 3	-----	----	----	----	----	----	----
22, 6 \pm 4, 8	-----	----	----	----	----	0, 097	0, 168
24, 0 \pm 5, 1	10, 5 \pm 1, 5	----	----	----	----	.083	.190

conditions

-----	-----	93, 6	90, 3	6, 3	803	0, 180	0, 291
10, 6 \pm 1, 9	-----	93, 3	88, 8	7, 3	421	.189	.308
18, 0 \pm 4, 1	-----	95, 3	90, 8	7, 6	650	.193	.386
-----	-----	94, 4	90, 2	6, 0	548	.190	.366
15, 0 \pm 3, 3	-----	94, 8	89, 9	5, 9	990	.212	.409
15, 0 \pm 3, 0	-----	94, 1	88, 4	8, 7	550	.210	.400
-----	-----	94, 2	89, 1	8, 1	859	.197	.501
-----	-----	94, 9	90, 2	6, 8	755	.199	.516
22, 5 \pm 4, 7	-----	93, 6	88, 3	7, 4	1144	.215	.512
22, 7 \pm 4, 3	-----	93, 6	90, 4	7, 4	537	.225	.579
20, 8 \pm 3, 8	-----	93, 4	88, 4	8, 9	742	.225	.561
-----	-----	94, 4	91, 7	6, 9	948	.196	.632
29, 6 \pm 5, 7	-----	93, 4	87, 6	6, 5	1482	.198	.635
28, 2 \pm 5, 3	-----	93, 3	84, 9	9, 9	1369	.197	.635
26, 4 \pm 5, 2	-----	93, 5	88, 7	5, 2	1410	.188	.597
28, 2 \pm 6, 1	-----	94, 1	88, 7	7, 2	1421	.193	.591
28, 1 \pm 6, 8	-----	93, 9	90, 5	7, 3	1481	.208	.657
27, 7 \pm 6, 2	-----	94, 2	87, 5	10, 6	1325	.215	.674
29, 1 \pm 6, 1	-----	92, 4	88, 0	6, 2	1278	.214	.631
29, 0 \pm 5, 8	-----	93, 2	88, 5	7, 1	696	.224	.678
28, 0 \pm 5, 3	-----	93, 5	88, 2	7, 5	1112	.217	.650
-----	-----	94, 2	88, 1	8, 1	1080	.203	.829
-----	-----	94, 0	90, 1	8, 0	1059	.201	.803
40, 2 \pm 7, 8	-----	93, 7	88, 5	8, 1	1650	.205	.789
38, 7 \pm 6, 6	-----	93, 3	88, 4	7, 5	2020	.233	.845
40, 0 \pm 7, 5	-----	94, 0	87, 7	7, 8	1459	.217	.867
39, 0 \pm 8, 3	-----	92, 3	87, 1	8, 3	1577	.219	.808
41, 6 \pm 7, 5	-----	92, 5	87, 1	6, 9	1090	.223	.883
38, 6 \pm 7, 0	-----	92, 9	86, 7	8, 4	1105	.215	.822
54, 1 \pm 8, 4	-----	93, 0	87, 8	6, 4	1131	.207	.988
-----	-----	93, 5	87, 4	9, 5	1324	.201	1, 00
-----	-----	91, 6	87, 4	9, 6	1479	.199	1, 03
-----	-----	91, 9	84, 2	9, 2	1572	.204	1, 02
51, 2 \pm 9, 3	-----	91, 5	83, 8	10, 4	1337	.216	1, 02
49, 4 \pm 9, 0	-----	91, 9	86, 0	8, 1	1311	.217	.989

TABLE V. - REGENERATOR PERFORMANCE - AXIAL-

(a) SI

Simulated gas generator speed, percent	Regenerator speed, rpm	High-pressure-side airflow, kg/sec	Low-pressure-side gas flow, kg/sec	Average cold-air temperature		Average hot-gas temperature	
				Inlet, t_c , in, °C	Outlet, t_c , out, °C ± σ	Inlet, t_h , in, °C	Outlet, t_h , out, °C ± σ
Ambient-flow							
---	----	0.531	0.531	Ambient	Ambient	Ambient	Ambient
Hot-flow test							
50	11.9	0.186	0.191	89	703±7	731	189±41
60	15.7	.242	.246	97	714±7	745	206±37
	15.7	.251	.278	96	704±5	731	246±50
70	19.1	.301	.309	110	687±6	723	220±36
	18.8	.302	.306	123	703±5	732	223±32
	18.7	.321	.338	119	707±4	734	246±39
80	20.7	.411	.420	137	676±4	711	253±34
	20.6	.446	.415	151	714±4	744	265±34
90	23.5	.497	.518	184	695±4	728	299±32
	23.4	.504	.517	178	697±4	724	287±31
100	23.1	.610	.632	213	668±6	703	313±29
	23.2	.607	.623	219	677±7	711	322±30

(b) U. S.

Simulated gas generator speed, percent	Regenerator speed, rpm	High-pressure-side airflow, lb/sec	Low-pressure-side gas flow, lb/sec	Average cold-air temperature		Average hot-gas temperature	
				Inlet, t_c , in, °F	Outlet, t_c , out, °F ± σ	Inlet, t_h , in, °F	Outlet, t_h , out, °F ± σ
Ambient-flow							
---	0	1.17	1.17	Ambient	Ambient	Ambient	Ambient
Hot-flow test							
50	11.9	0.409	0.420	192	1297±12	1349	372±73
60	15.7	.534	.542	213	1317±12	1373	402±67
	15.7	.553	.612	204	1300±9	1347	475±90
70	19.1	.664	.681	230	1269±11	1334	428±64
	18.8	.665	.674	253	1297±9	1351	434±57
	18.7	.708	.745	246	1305±8	1353	475±70
80	20.7	.907	.927	279	1249±8	1312	488±61
	20.6	.893	.915	303	1317±7	1372	509±61
90	23.5	1.095	1.141	364	1283±7	1342	571±57
	23.4	1.111	1.139	352	1286±8	1336	549±55
100	23.1	1.345	1.393	416	1235±11	1297	596±52
	23.2	1.339	1.373	427	1251±12	1312	612±54

FLOW HOUSING WITH 50 PERCENT BLOCKAGE

units

Low-pressure-side average gas velocity, m/sec $\pm \sigma$	High-pressure-side average air velocity, m/sec $\pm \sigma$	Temperature effectiveness for heating cold fluid, percent	Heat transfer effectiveness, percent	Leakage, percent of airflow	Torque, N-m	High-pressure-side pressure differential, kN/m ²	Low-pressure-side pressure differential, kN/m ²
test conditions							
6.6 \pm 1.3	3.3 \pm 1.6	----	----	----	----	----	----
conditions							
4.3 \pm 2.4	-----	95.4	90.2	6.9	45	1.34	2.28
5.2 \pm 1.3	-----	95.2	88.4	8.8	50	1.43	2.98
6.0 \pm 1.4	-----	95.9	88.3	5.8	56	1.65	3.56
6.4 \pm 1.7	-----	94.2	87.8	7.6	75	1.42	3.56
7.2 \pm 2.0	-----	95.1	88.1	7.8	68	1.45	3.53
8.2 \pm 2.1	-----	95.6	87.0	10.7	89	1.59	4.24
9.7 \pm 1.8	4.1 \pm 2.1	93.9	85.2	10.7	93	1.50	4.87
10.4 \pm 2.8	-----	94.9	86.5	11.6	119	1.57	5.04
13.4 \pm 3.1	-----	94.1	86.1	9.5	132	1.59	6.19
13.9 \pm 3.3	-----	94.8	85.8	10.6	152	1.52	6.13
16.9 \pm 3.6	-----	93.0	86.3	9.9	144	1.52	7.03
-----	-----	93.1	85.4	11.7	142	1.52	7.10

customary units

Low-pressure-side average gas velocity, ft/sec $\pm \sigma$	High-pressure-side average air velocity, ft/sec $\pm \sigma$	Temperature effectiveness for heating cold fluid, percent	Heat transfer effectiveness, percent	Leakage, percent of airflow	Torque, in-lb	High-pressure-side pressure differential, psi	Low-pressure-side pressure differential, psi
test conditions							
21.7 \pm 4.3	10.7 \pm 5.2	----	----	----	----	----	----
conditions							
14.0 \pm 7.8	-----	95.4	90.2	6.9	395	0.194	0.331
17.1 \pm 4.4	-----	95.2	88.4	8.8	444	.208	.432
19.7 \pm 4.7	-----	95.9	88.3	5.8	492	.240	.516
20.9 \pm 5.7	-----	94.2	87.8	7.6	658	.206	.517
23.5 \pm 6.4	-----	95.1	88.1	7.8	598	.211	.512
26.8 \pm 6.9	-----	95.6	87.0	10.7	786	.230	.615
31.8 \pm 5.9	13.5 \pm 6.9	93.9	85.2	10.7	819	.218	.706
34.2 \pm 9.1	-----	94.9	86.5	11.6	1047	.228	.731
44.1 \pm 10.2	-----	94.1	86.1	9.5	1161	.231	.898
45.6 \pm 10.8	-----	94.8	85.8	10.6	1333	.220	.889
55.4 \pm 11.7	-----	93.0	86.3	9.9	1267	.221	1.02
-----	-----	93.1	85.4	11.7	1249	.220	1.03

TABLE VI. - REGENERATOR

(a) SI

Condition (70 percent gas generator speed)	Regenerator speed, rpm	High-pressure-side airflow, kg/sec	Low-pressure-side gas flow, kg/sec	Average cold-air temperature		Average hot-gas temperature	
				Inlet, t_c , in, °C	Outlet, t_c , out, °C $\pm \sigma$	Inlet, t_h , in, °C	Outlet, t_h , out, °C $\pm \sigma$
32 min before failure	18.8	0.320	0.329	118	709 \pm 4	744	221 \pm 31
20 min before failure	20.0	.227	.345	69	716 \pm 5	746	366 \pm 72
10 min before failure	20.0	.177	.345	53	713 \pm 4	747	438 \pm 83
6 min before failure	20.0	.172	.345	49	-----	733	-----
At failure	20.0	.454	.454	38	-----	738	-----

(b) U. S.

Condition (70 percent gas generator speed)	Regenerator speed, rpm	High-pressure-side airflow, lb/sec	Low-pressure-side gas flow, lb/sec	Average cold-air temperature		Average hot-gas temperature	
				Inlet, t_c , in, °F	Outlet, t_c , out, °F $\pm \sigma$	Inlet, t_h , in, °F	Outlet, t_h , out, °F $\pm \sigma$
32 min before failure	18.8	0.706	0.726	244	1309 \pm 8	1372	429 \pm 56
20 min before failure	20.0	.500	.760	157	1320 \pm 9	1375	690 \pm 129
10 min before failure	20.0	.390	.760	128	1315 \pm 8	1377	821 \pm 150
6 min before failure	20.0	.380	.760	120	-----	1352	-----
At failure	20.0	1.000	1.000	100	-----	1360	-----

FAILURE DATA

units

Low-pressure-side inlet pressure, kN/m ²	High-pressure-side inlet pressure, kN/m ²	Temperature effectiveness for heating cold fluid, percent	Heat transfer effectiveness, percent	Leakage, percent of airflow	Torque, N-m	High-pressure-side pressure differential, kN/m ²	Low-pressure-side pressure differential, kN/m ²
103.4	210.3	94.4	91.5	8.3	76	1.53	3.69
104.8	153.1	95.5	92.9	8.3	39	1.94	5.12
106.2	131.7	95.0	94.2	12.2	34	1.78	5.45
103	131.7	----	----	----	23	----	----
103	408.2	----	----	----	113	----	----

customary units

Low-pressure-side inlet pressure, psia	High-pressure-side inlet pressure, psia	Temperature effectiveness for heating cold fluid, percent	Heat transfer effectiveness, percent	Leakage, percent of airflow	Torque, in-lb	High-pressure-side pressure differential, psi	Low-pressure-side pressure differential, psi
15.0	30.5	94.4	91.5	8.3	668	0.222	0.535
15.2	22.2	95.5	92.9	8.3	345	.282	.743
15.4	19.1	95.0	94.2	12.2	300	.259	.791
≈15	19.1	----	----	----	200	----	----
≈15	59.2	----	----	----	990	----	----

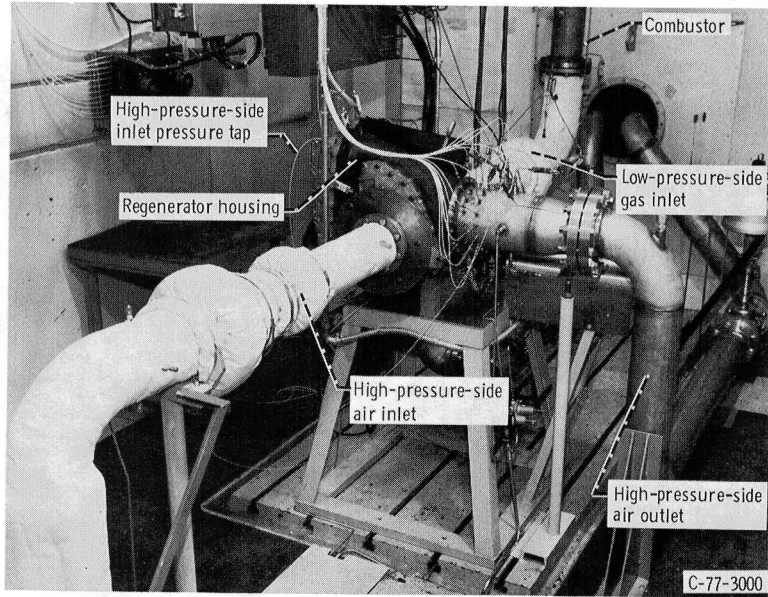
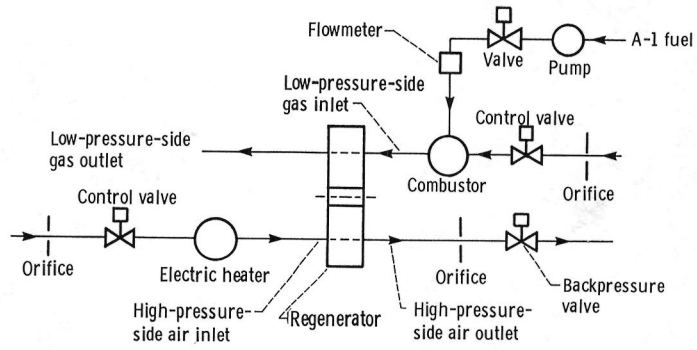


Figure 1. - Regenerator system test facility.

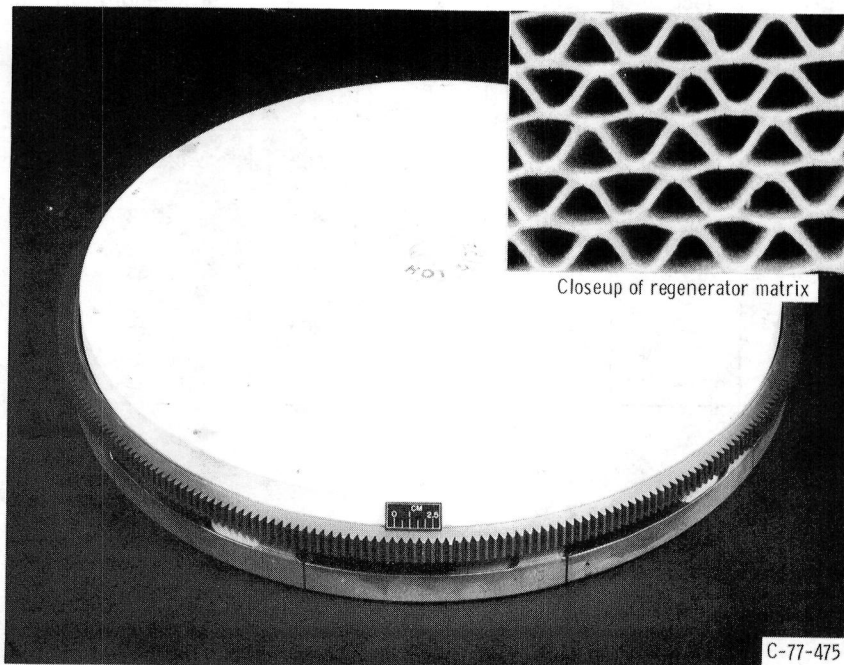


Figure 2. - Regenerator core with ring drive gear.

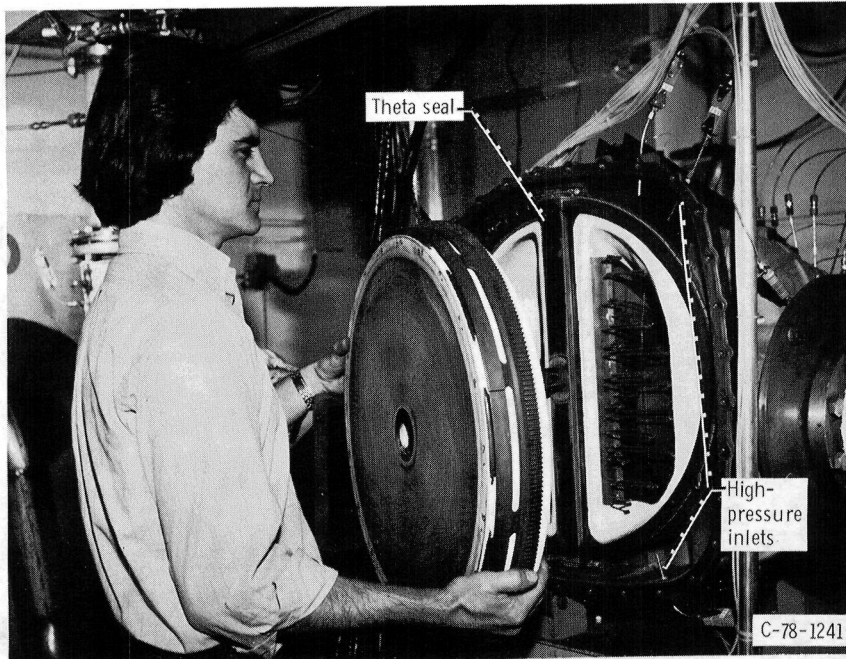


Figure 3. - Engine housing with regenerator core.

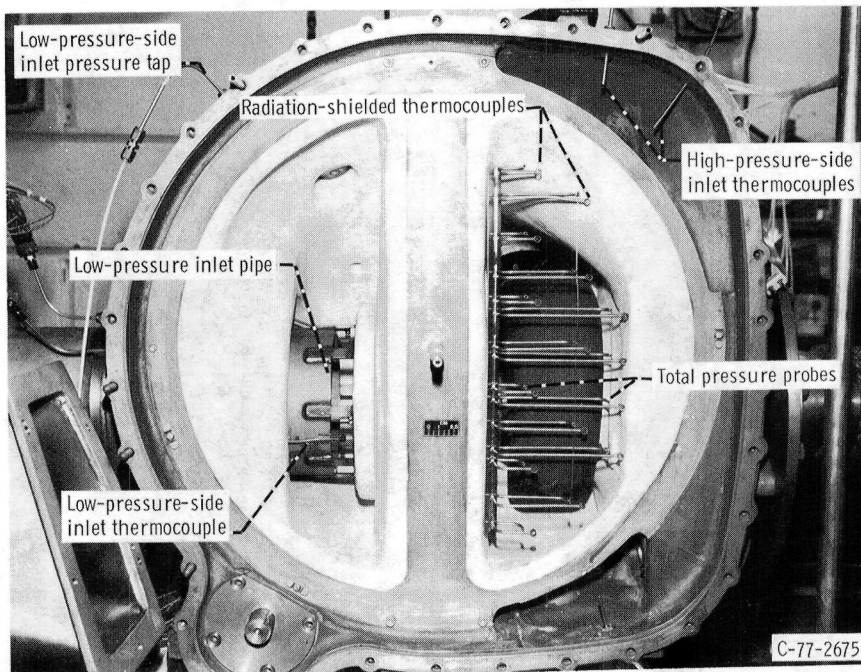


Figure 4. - Engine housing.

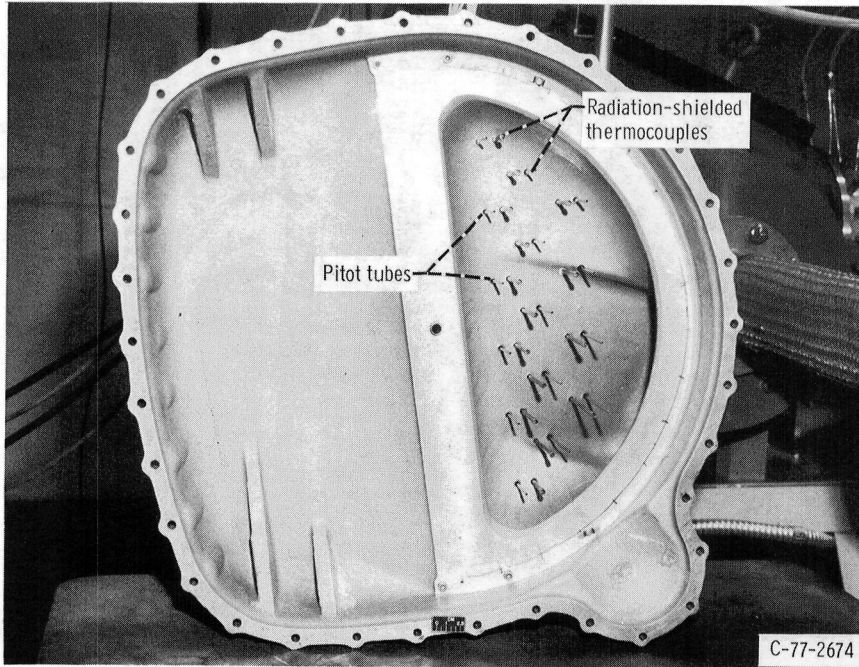


Figure 5. - Engine housing regenerator cover.

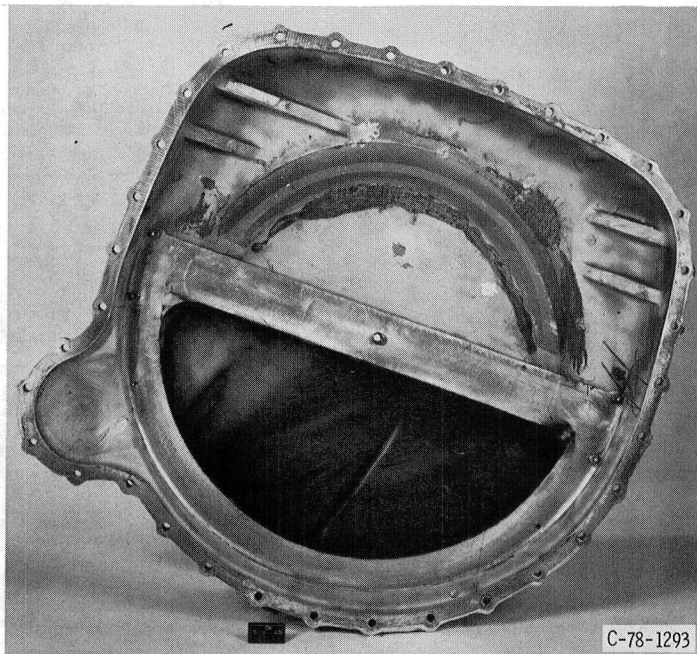


Figure 6. - Engine housing regenerator cover with baffle installed.

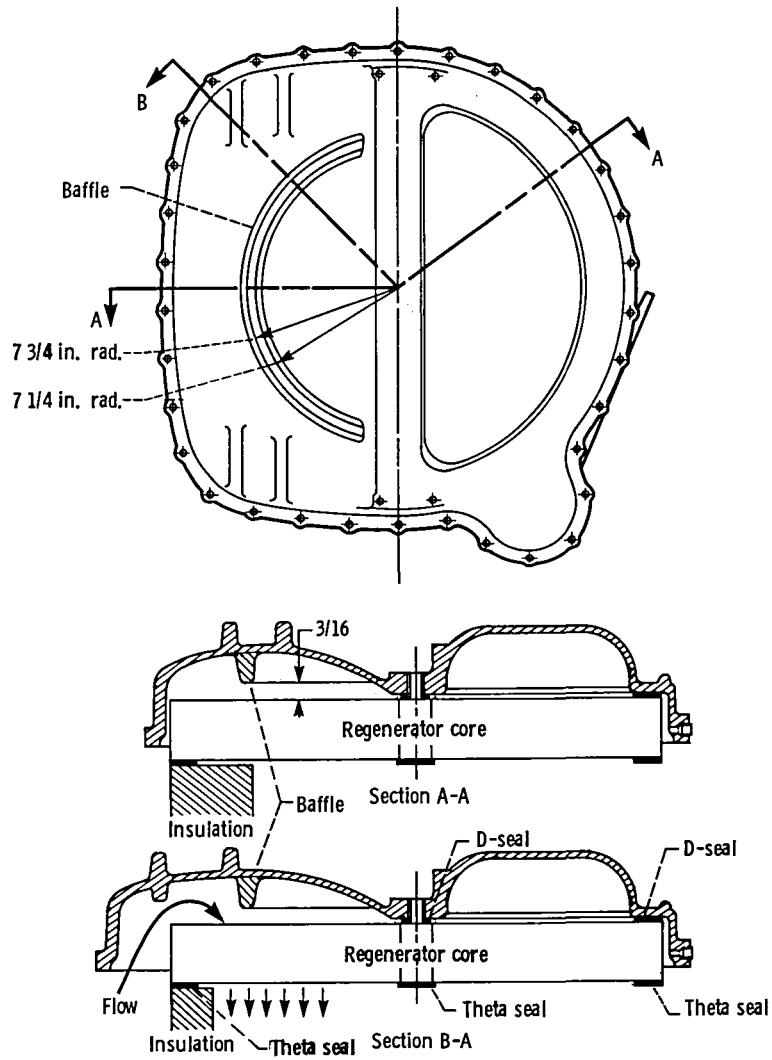


Figure 7. - Details of regenerator cover with baffle installed.

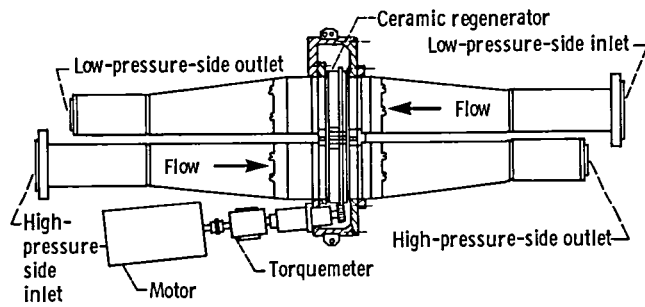
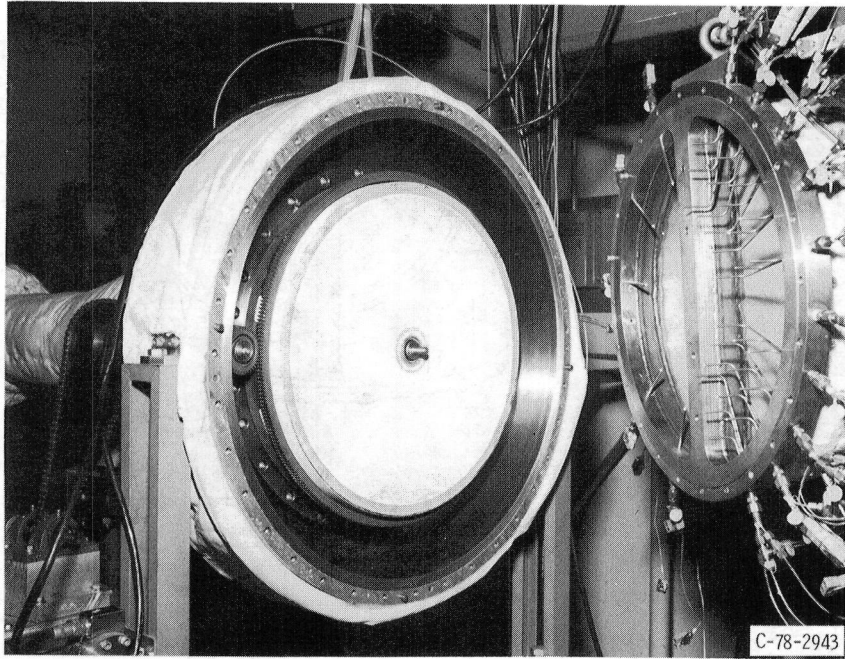
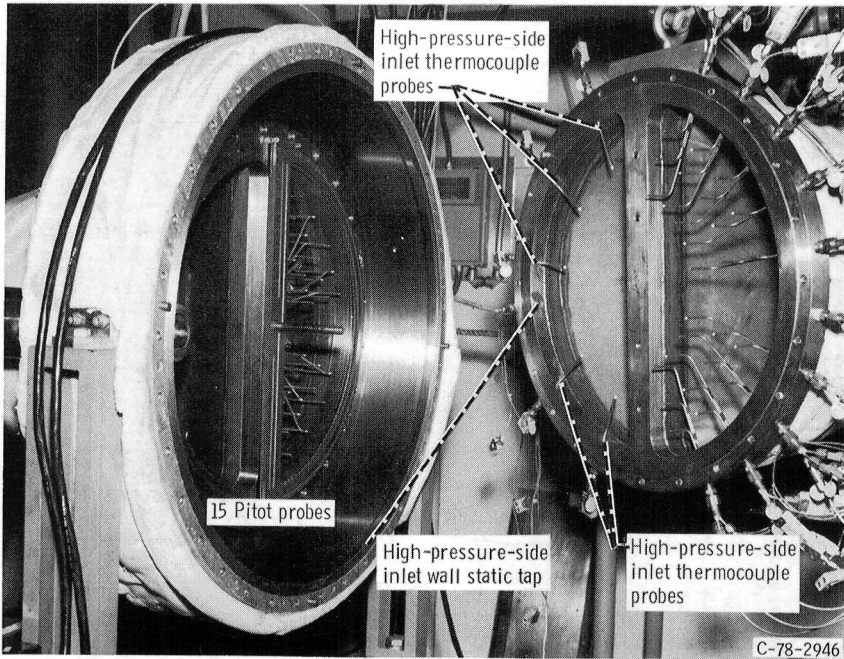


Figure 8. - Axial-flow housing.



(a) With regenerator.



(b) Without regenerator.

Figure 9. - Axial-flow housing.

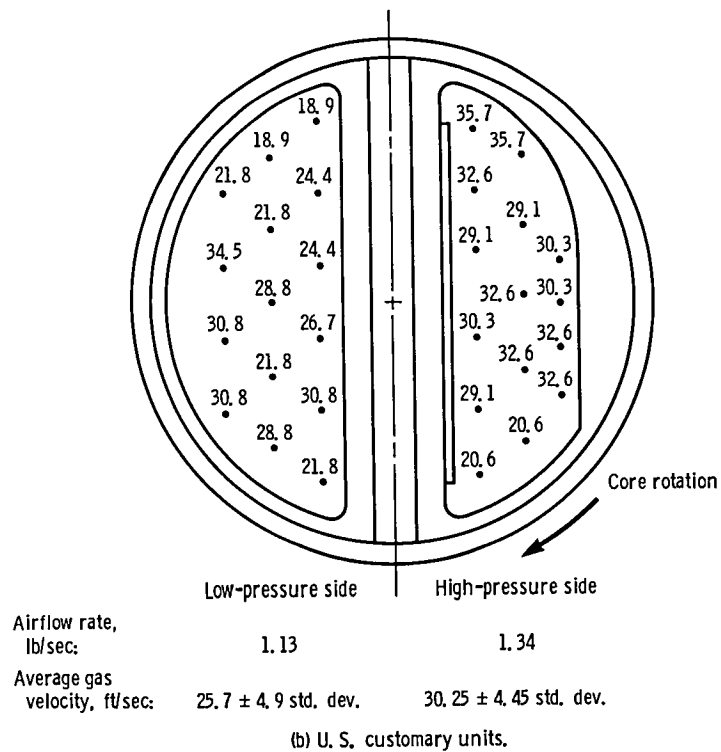
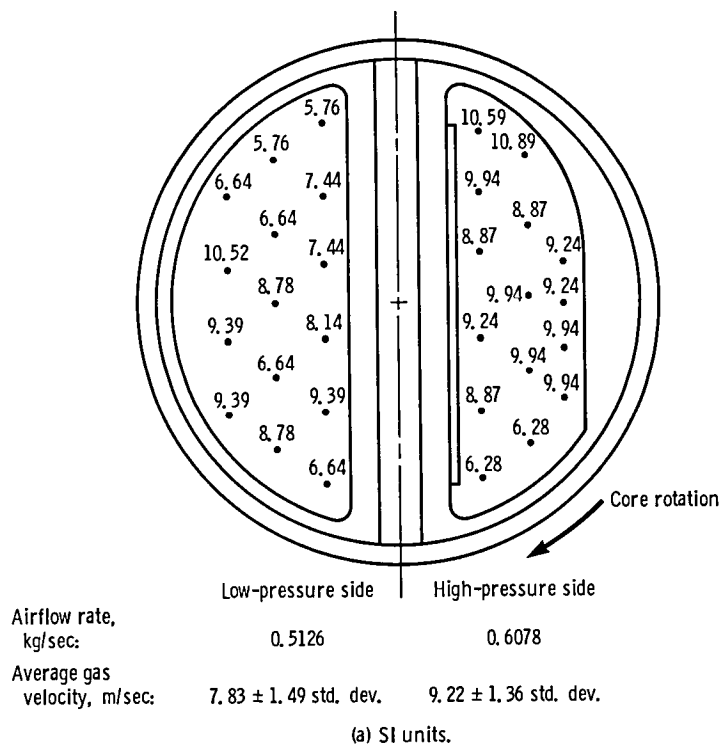


Figure 10. - Velocity data for ambient-temperature flow - engine housing with original core.

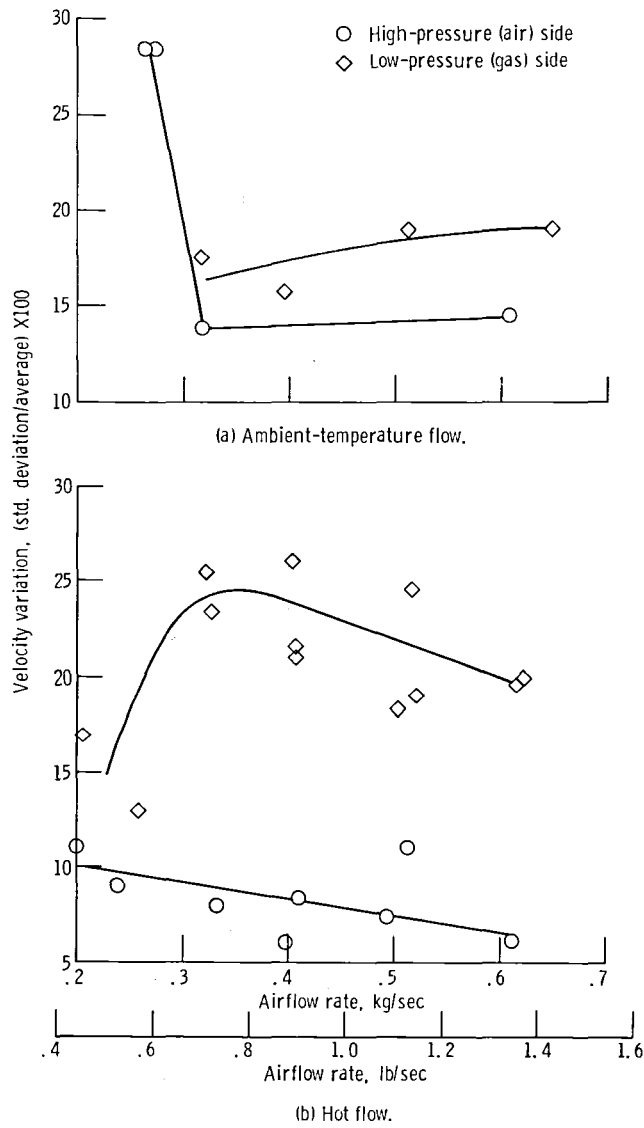
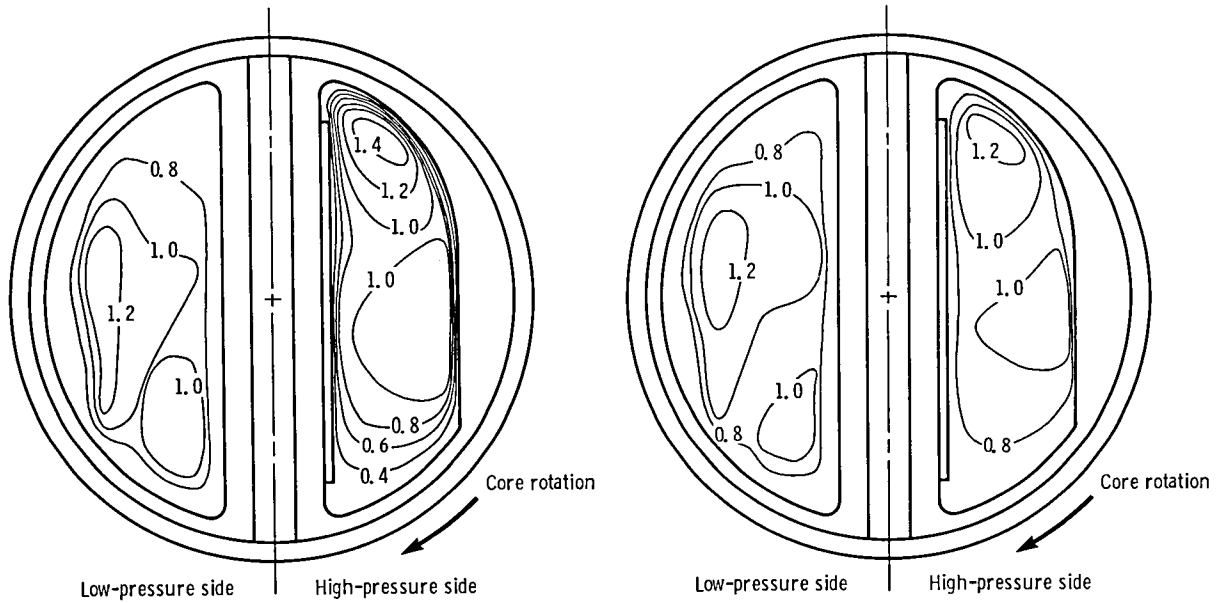


Figure 11. - Velocity uniformity - engine housing with original cover.

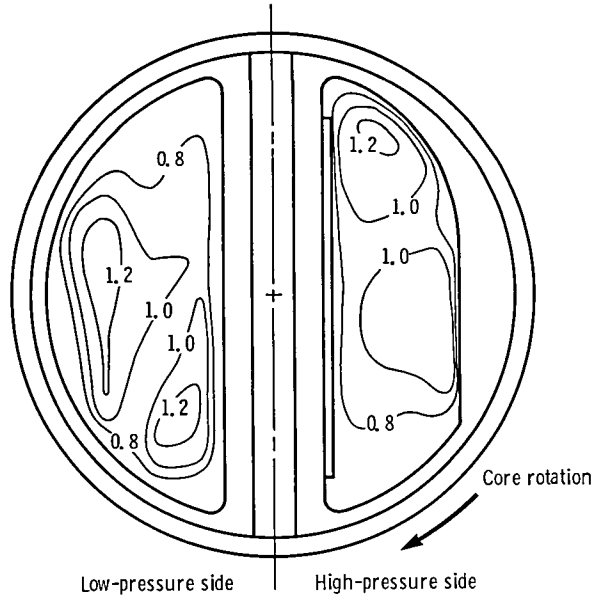


Airflow rate, kg/sec (lb/sec):	0.395 (0.87)	0.272 (0.60)
Average gas velocity, m/sec (ft/sec):	9.57 (31.4) ± 19%	6.49 (21.3) ± 28%

Airflow rate, kg/sec (lb/sec):	0.317 (0.70)	0.317 (0.70)
Average gas velocity, m/sec (ft/sec):	4.88 (16.0) ± 17%	8.56 (28.1) ± 14%

(a) 60, 70, and 80 Percent of simulated gas generator speed.

(b) 100 Percent of simulated gas generator speed.



Airflow rate, kg/sec (lb/sec):	0.513 (1.13)	0.608 (1.34)
Average gas velocity, m/sec (ft/sec):	7.83 (25.7) ± 19%	9.24 (30.3) ± 14%

(c) Maximum facility flow rate. $W_{HP} = 1.34$ lb/sec, $V_{avg} = 30.1$ ft/sec; $W_{LP} = 1.13$ lb/sec, $V_{avg} = 25.7$ ft/sec.

(c) Maximum flow rate.

Figure 12. - Ambient-flow velocity map - engine housing with original cover.

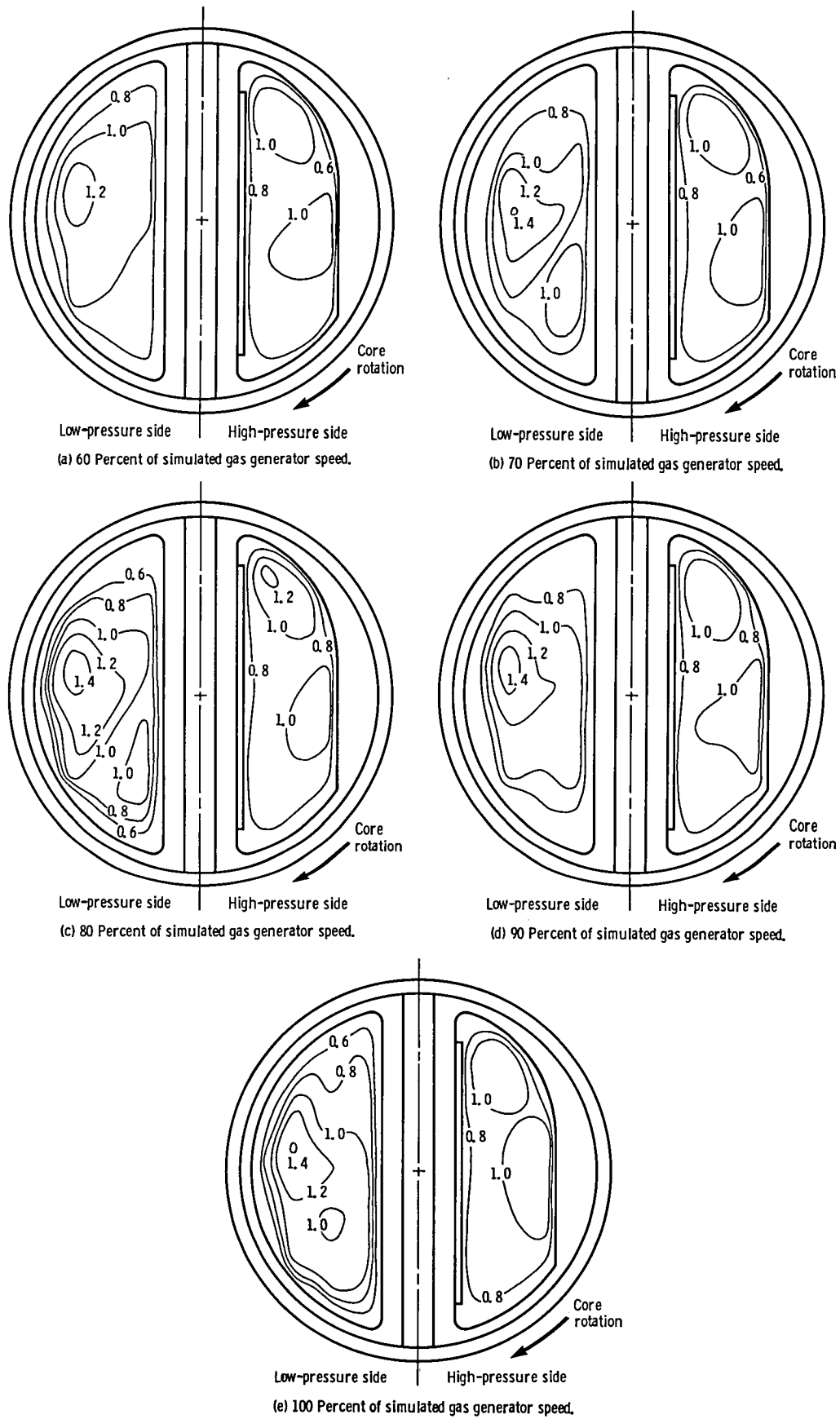
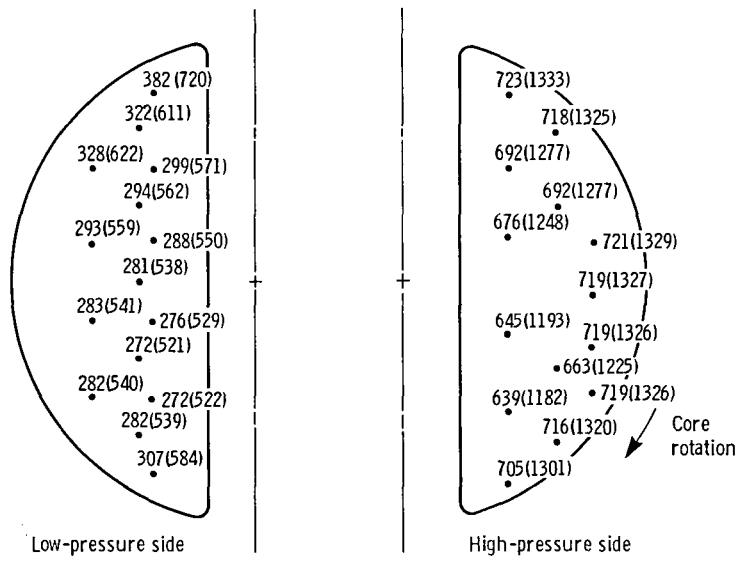


Figure 13. - Velocity map - engine housing with original cover.



Average temperature, °C (°F): 297.4 (567.3)

696.1 (1284.9)

Standard deviation, ±°C (°F): ±11.1 (± 51.9)

±11.7 (± 53.1)

Figure 14. - Temperature data for 100 percent of simulated gas generator speed - engine housing with original cover.

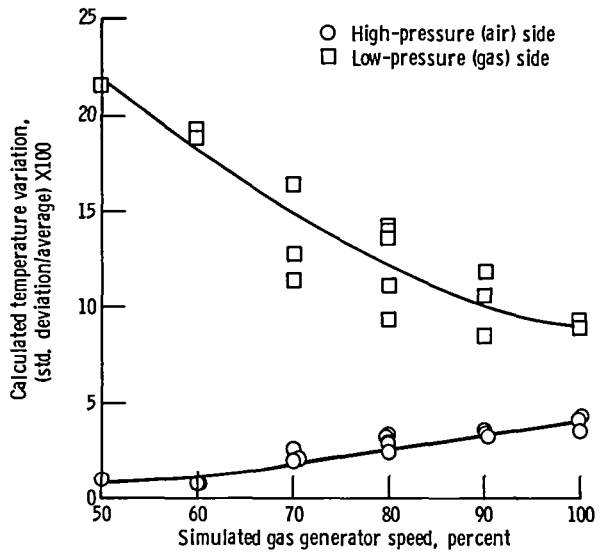
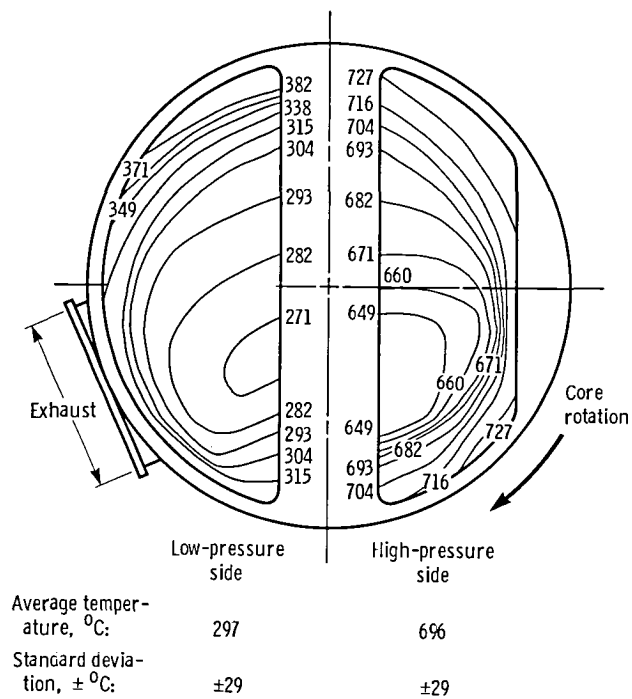
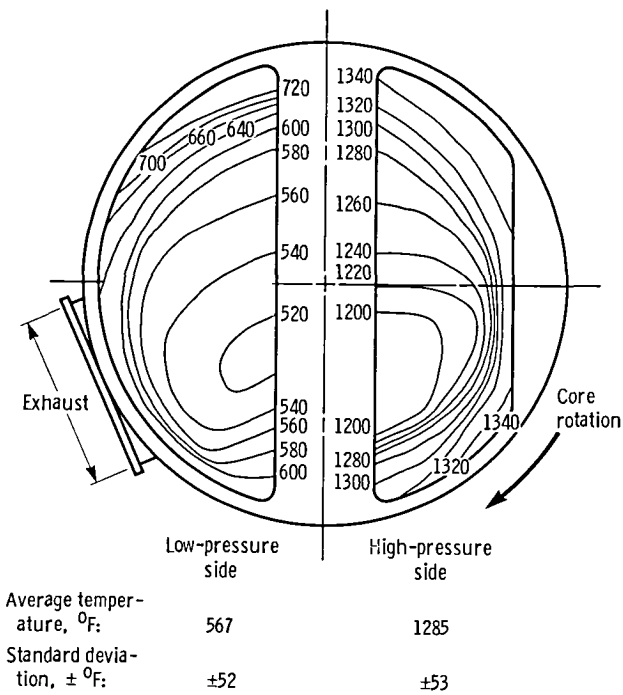


Figure 15. - Temperature output uniformity - engine housing with original cover.



(a) SI units.



(b) U. S. customary units.

Figure 16. - Temperature map for 100 percent of design speed - engine housing with original cover.

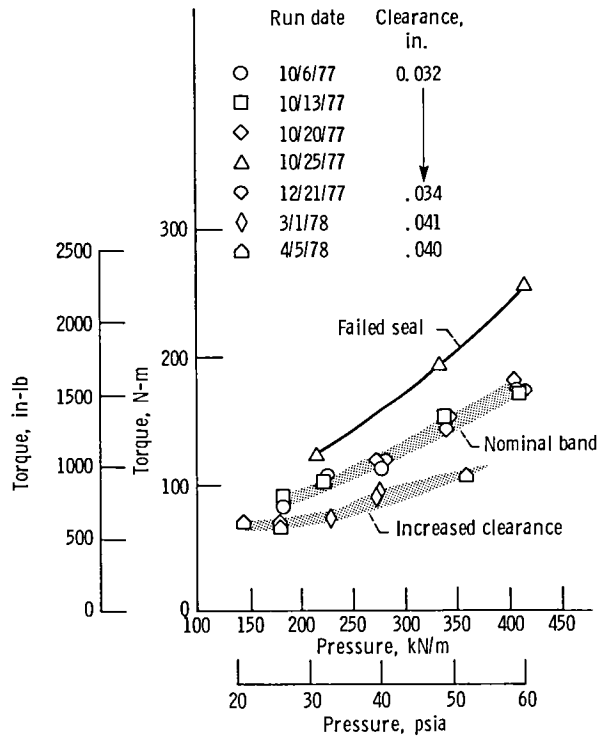


Figure 17. - Measured torque - engine housing with original cover.

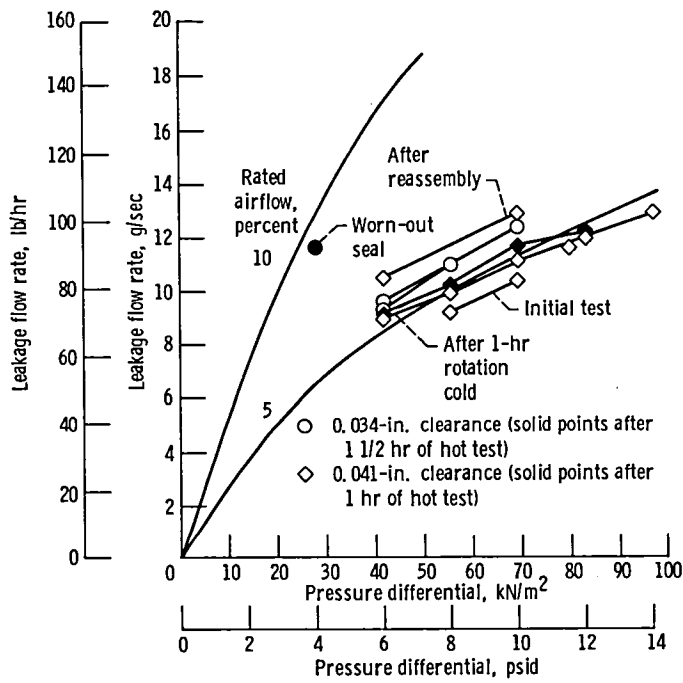


Figure 18. - Measured cold, static leakage - engine housing with original cover.

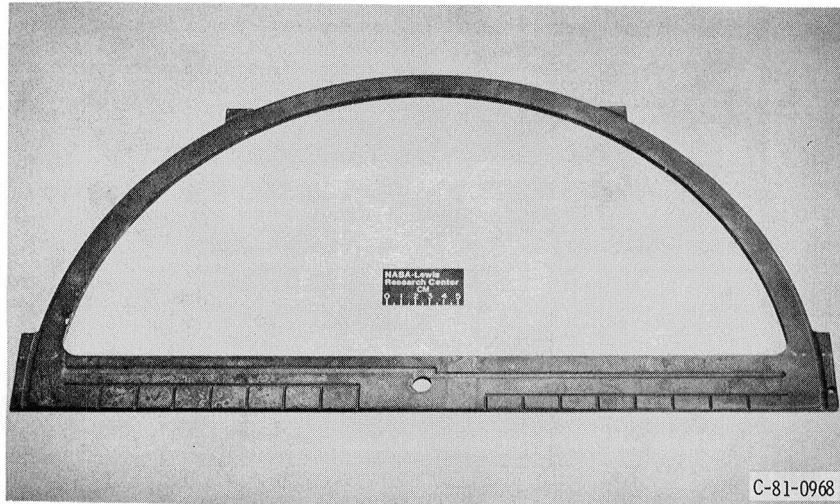


Figure 19. - Graphite polyimide D seal.

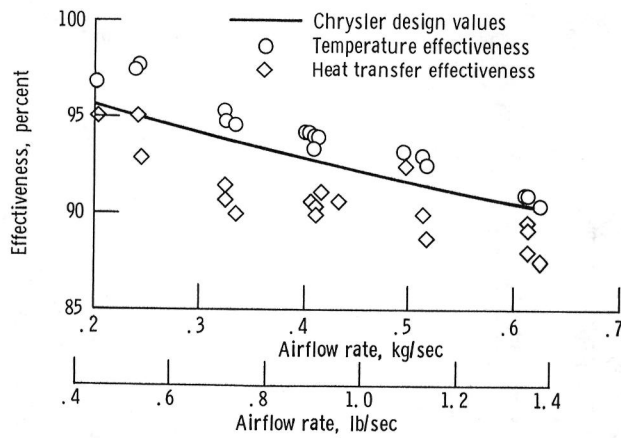


Figure 20. - Regenerator effectiveness measured in test facility - engine housing with original cover.

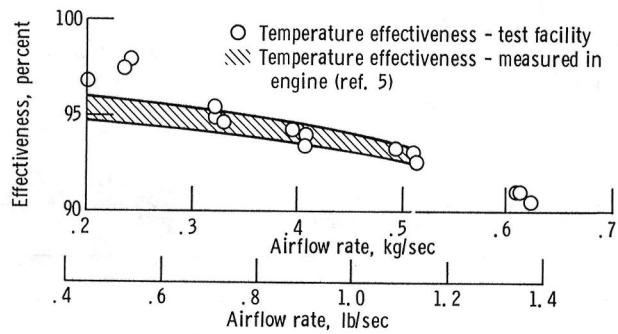


Figure 21. - Regenerator temperature effectiveness measured in test facility and in actual engine testing - engine housing with original cover.

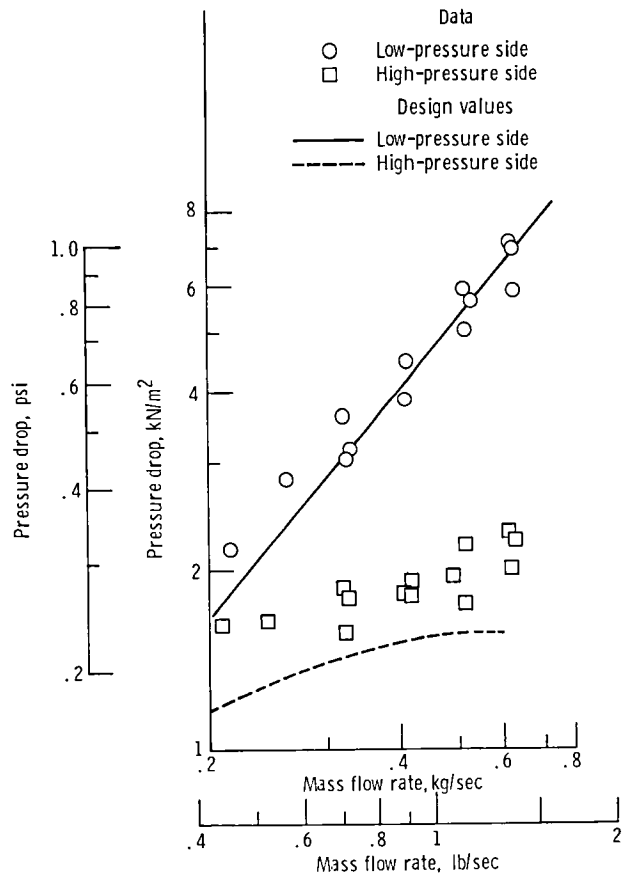


Figure 22. - Regenerator pressure drop - engine housing with original cover.

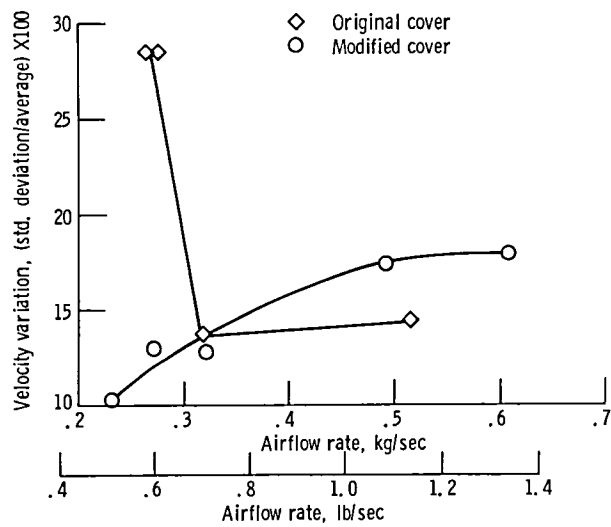


Figure 23. - Velocity uniformity for ambient-temperature flow - engine housing with original and modified covers.

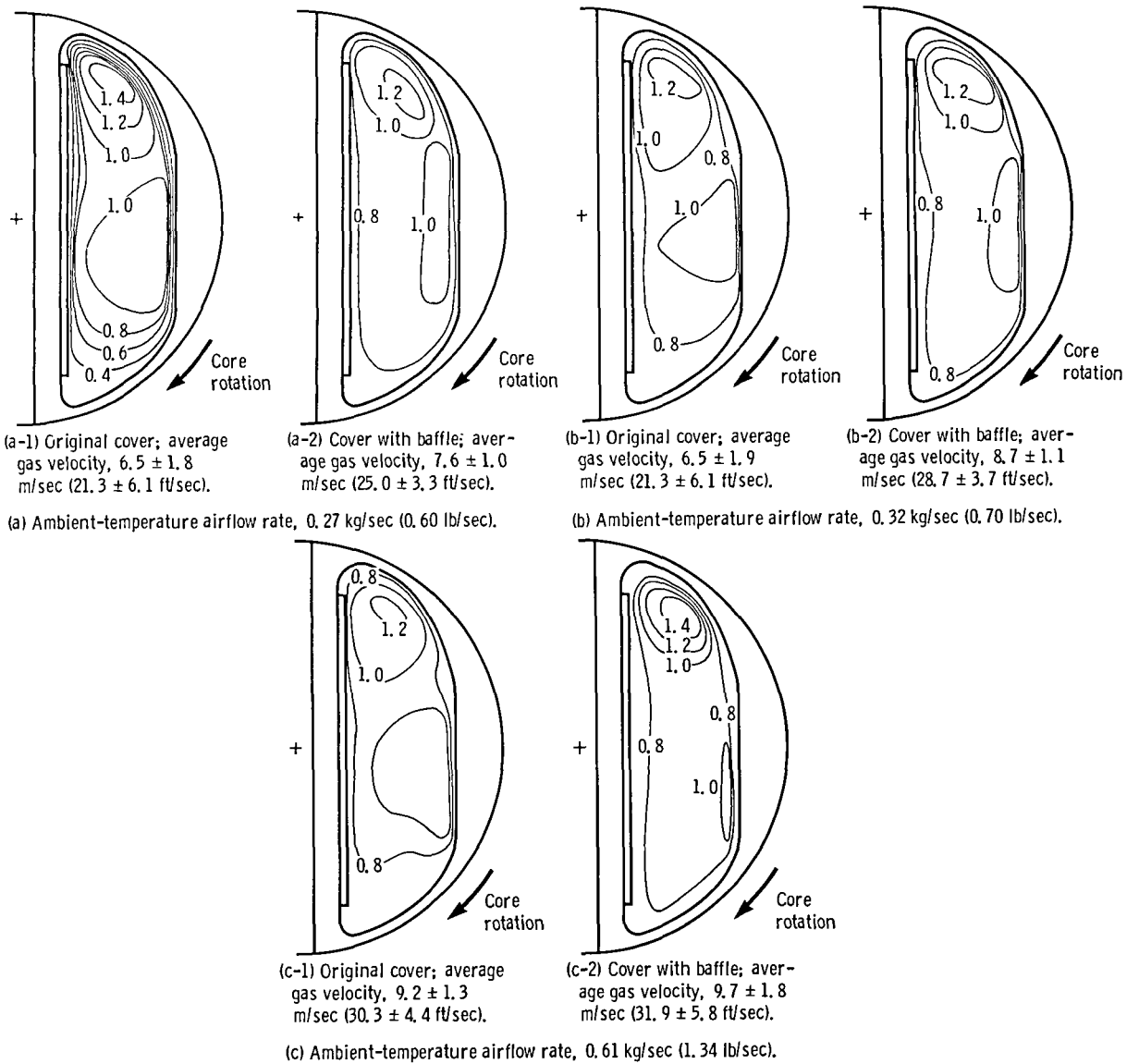


Figure 24. - High-pressure-side velocity map - engine housing with original and modified covers.

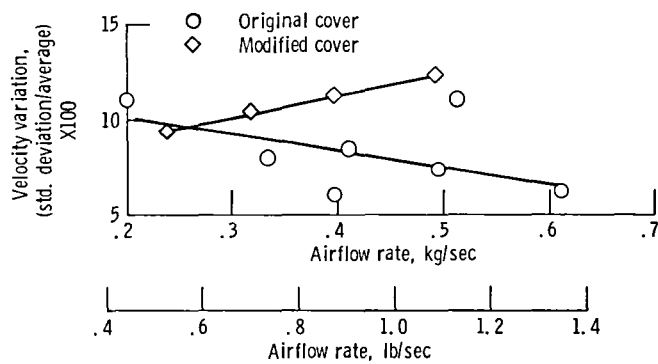


Figure 25. - High-pressure-side velocity uniformity for hot flow - engine housing with original and modified covers.

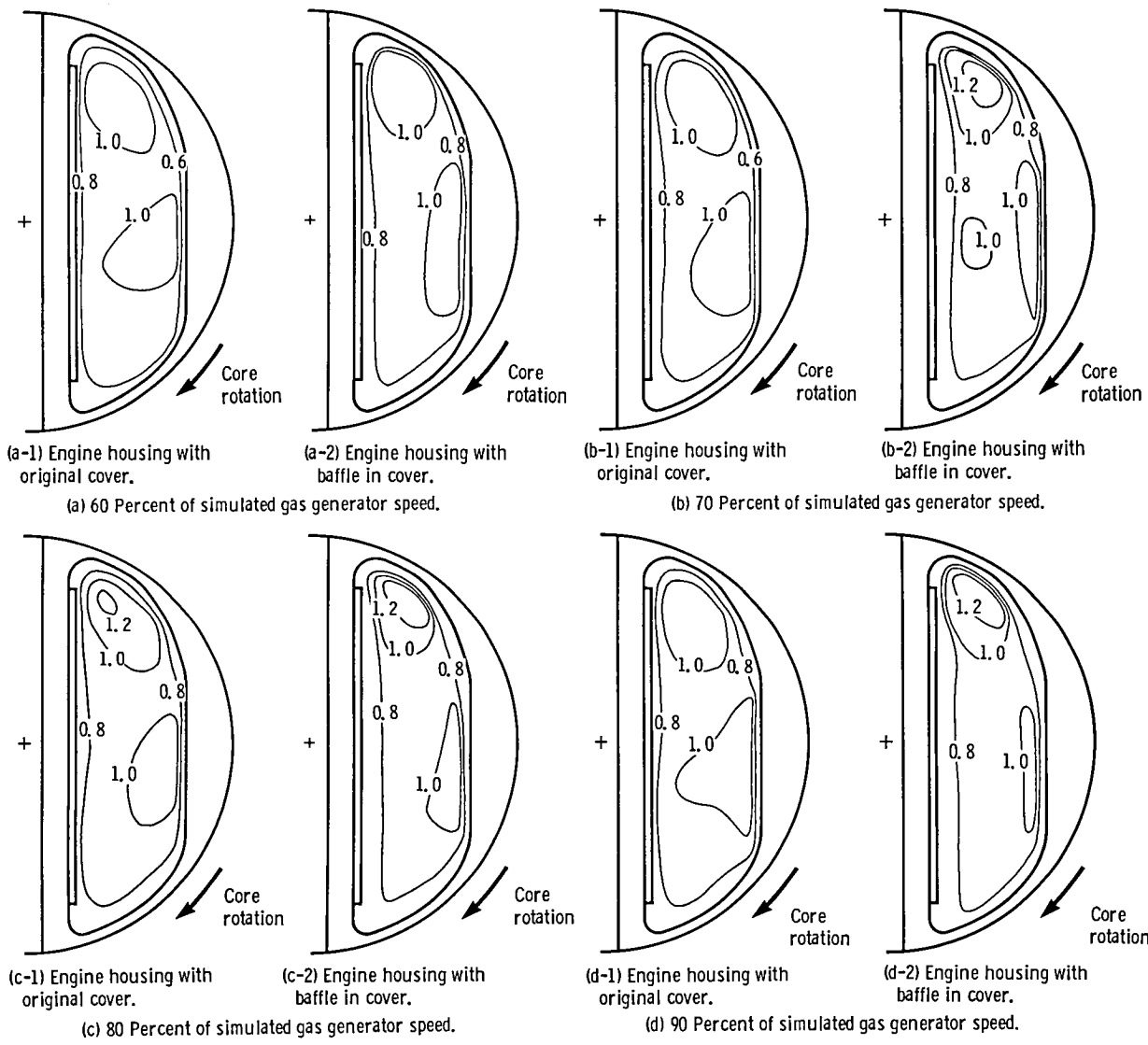


Figure 26. - High-pressure-side velocity map.

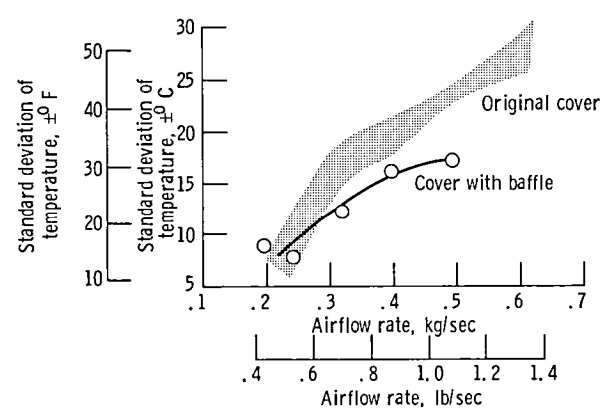


Figure 27. - High-pressure-side temperature output uniformity - engine housing with original and modified covers.

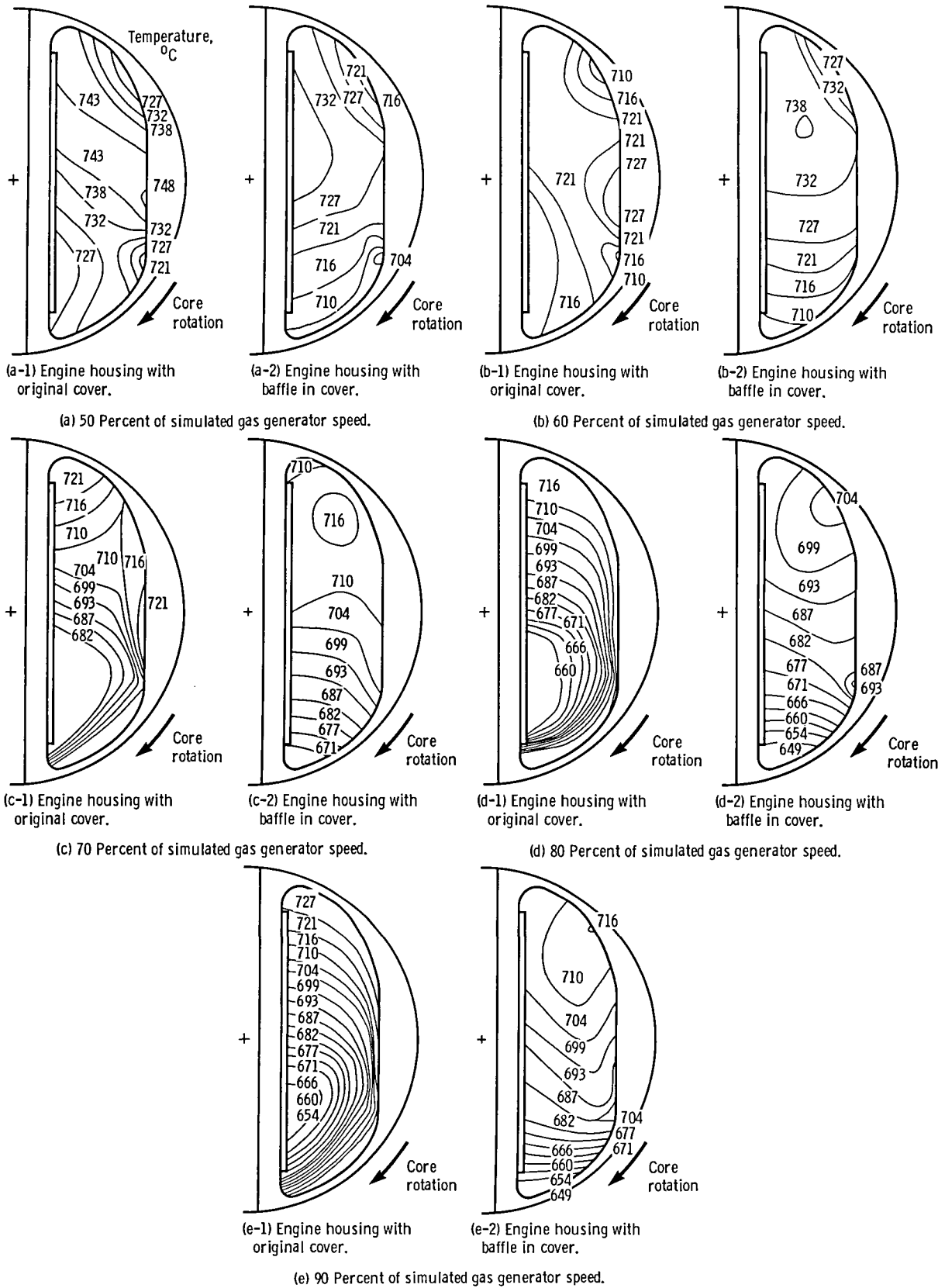


Figure 28. - High-pressure-side temperature map - SI units.

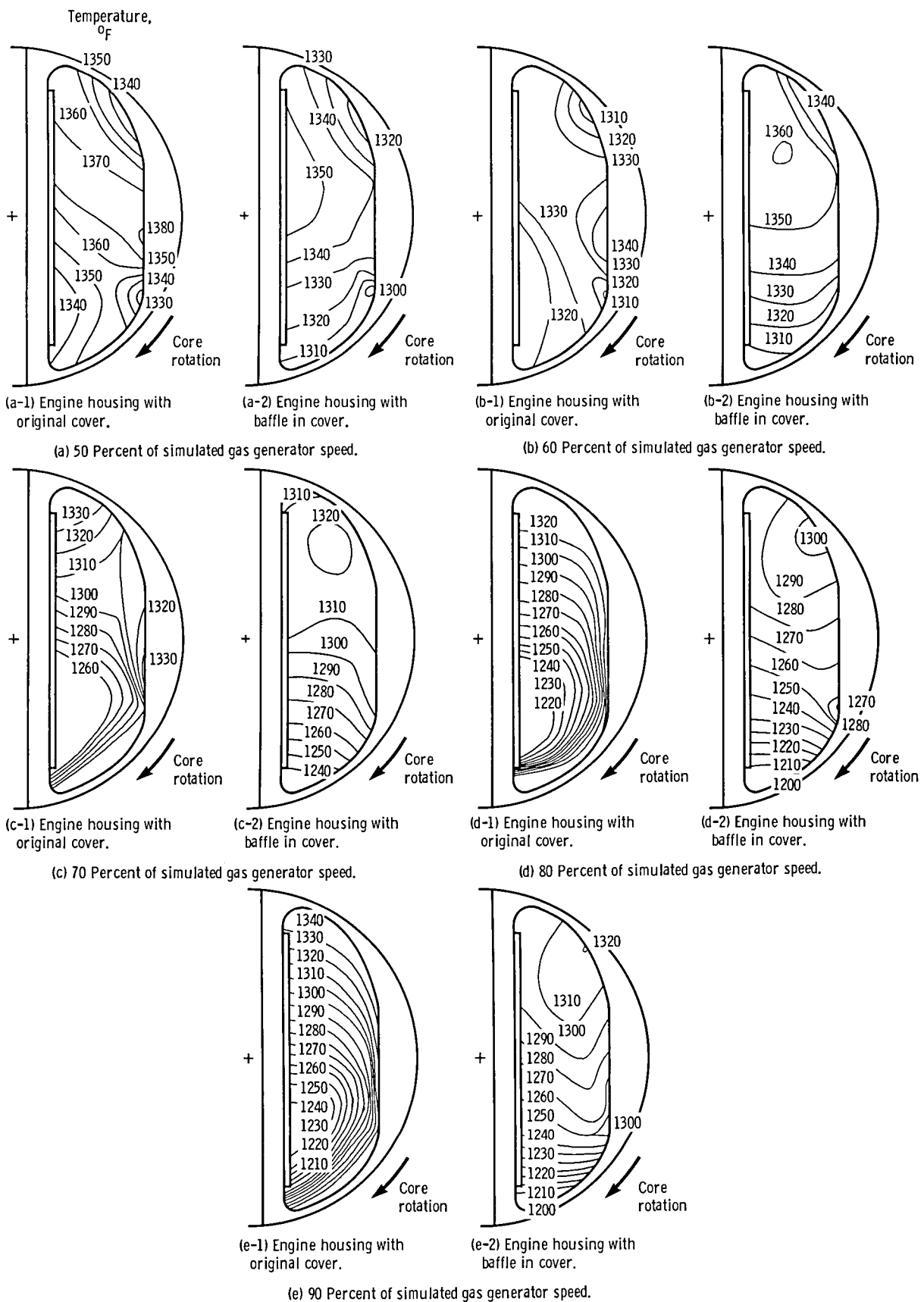


Figure 29. - High-pressure-side temperature map - U. S. customary units.

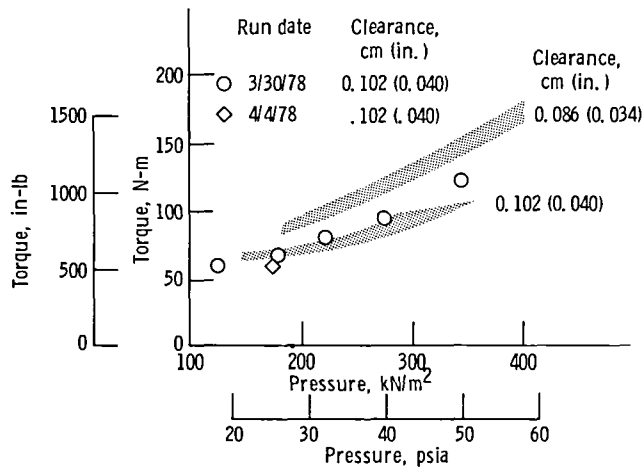


Figure 30. - Measured torque - engine housing with baffle in cover.

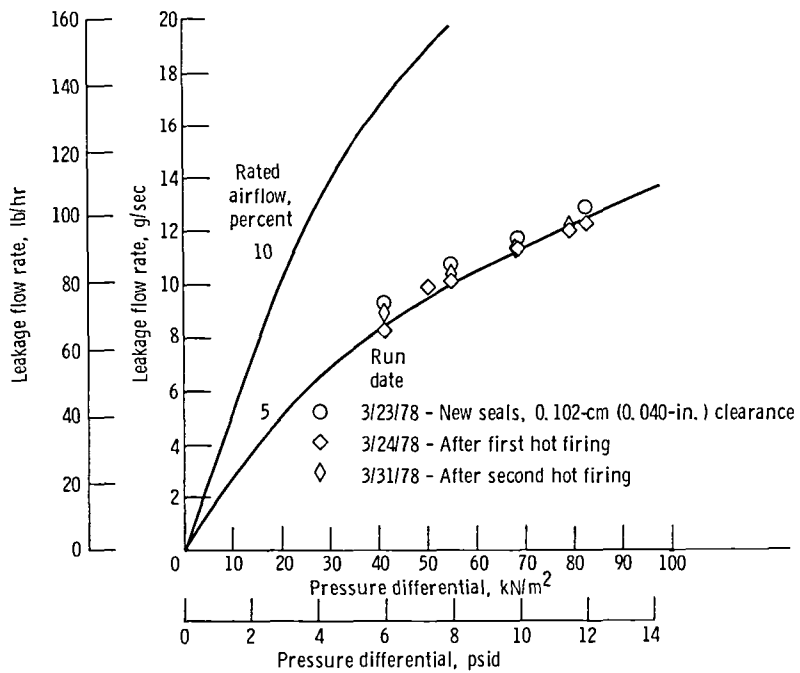


Figure 31. - Measured cold, static leakage - engine housing with baffle in cover.

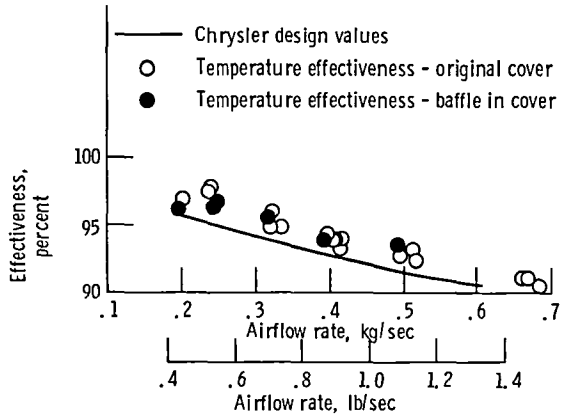


Figure 32. - Regenerator temperature effectiveness - engine housing with original and modified covers.

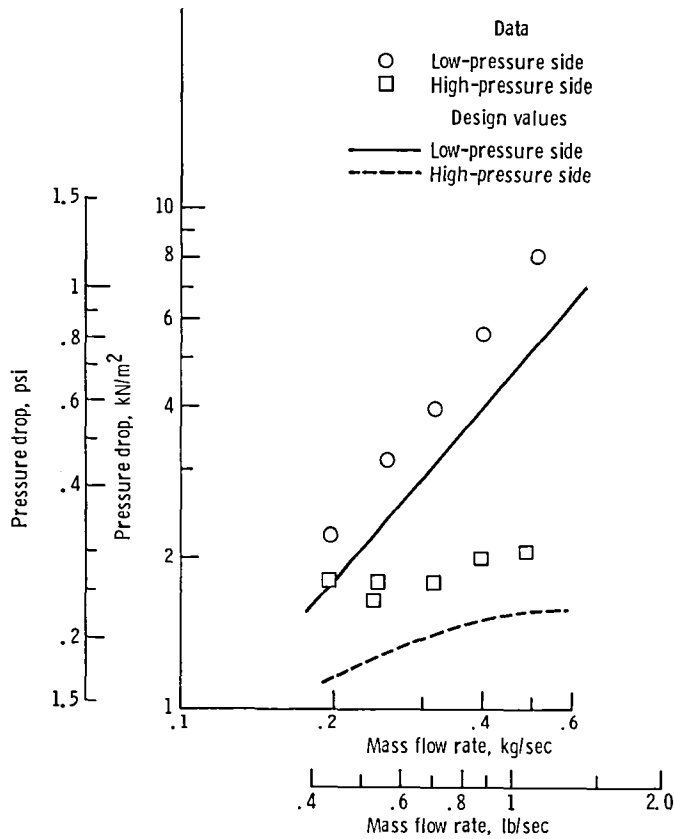
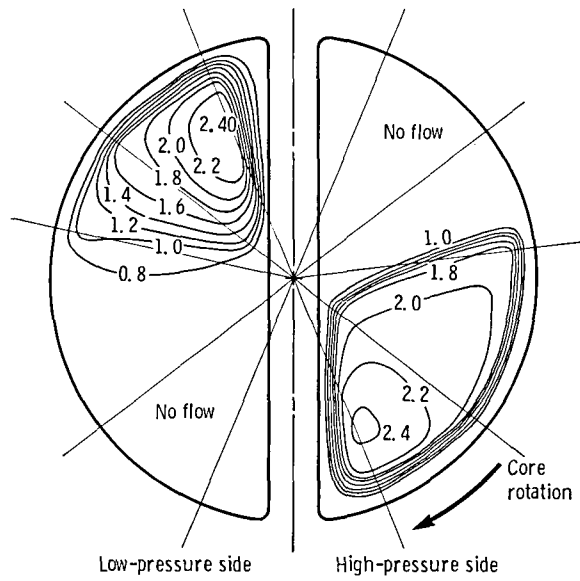
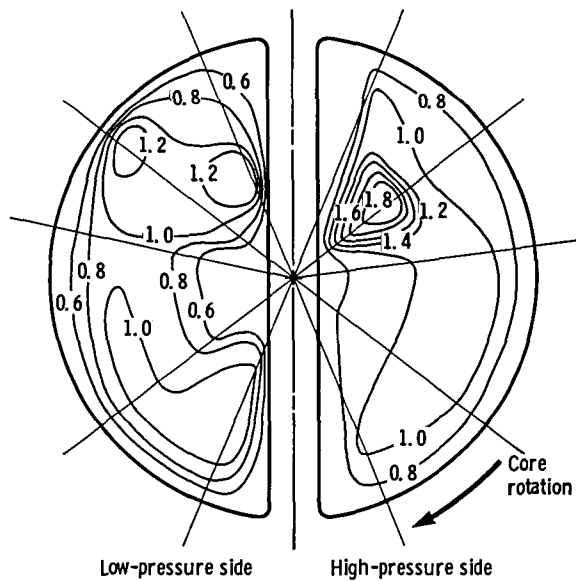


Figure 33. - Regenerator pressure drop - engine housing with baffle in cover.



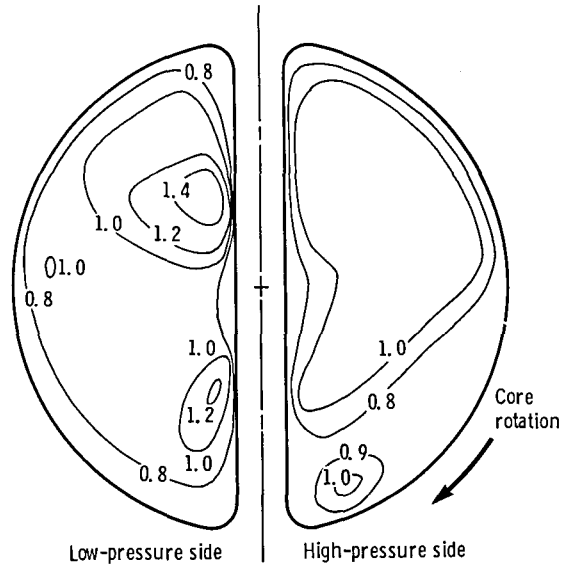
Average gas velocity,
 m/sec (ft/sec): 5.5 (18.2) 3.5 (11.4)

Figure 34. - Velocity map - axial-flow housing without regenerator. Airflow rate, 1.80 kg/sec (0.82 lb/sec); ambient-temperature flow.



Average gas velocity,
 m/sec (ft/sec): 6.1 (20.0) 4.3 (14.1)

Figure 35. - Velocity map - axial-flow housing with regenerator in place. Airflow rate, 1.80 kg/sec (0.82 lb/sec); ambient-temperature flow.



Airflow rate,		
kg/sec (lb/sec):	2.88 (1.31)	3.12 (1.42)
Average gas velocity,		
m/sec (ft/sec):	7.3 ± 1.6 (24.0 \pm 5.1)	3.2 ± 0.5 (10.5 \pm 1.5)

Figure 36. - Velocity map - axial-flow housing without regenerator. Maximum facility flow rate; ambient-temperature flow.

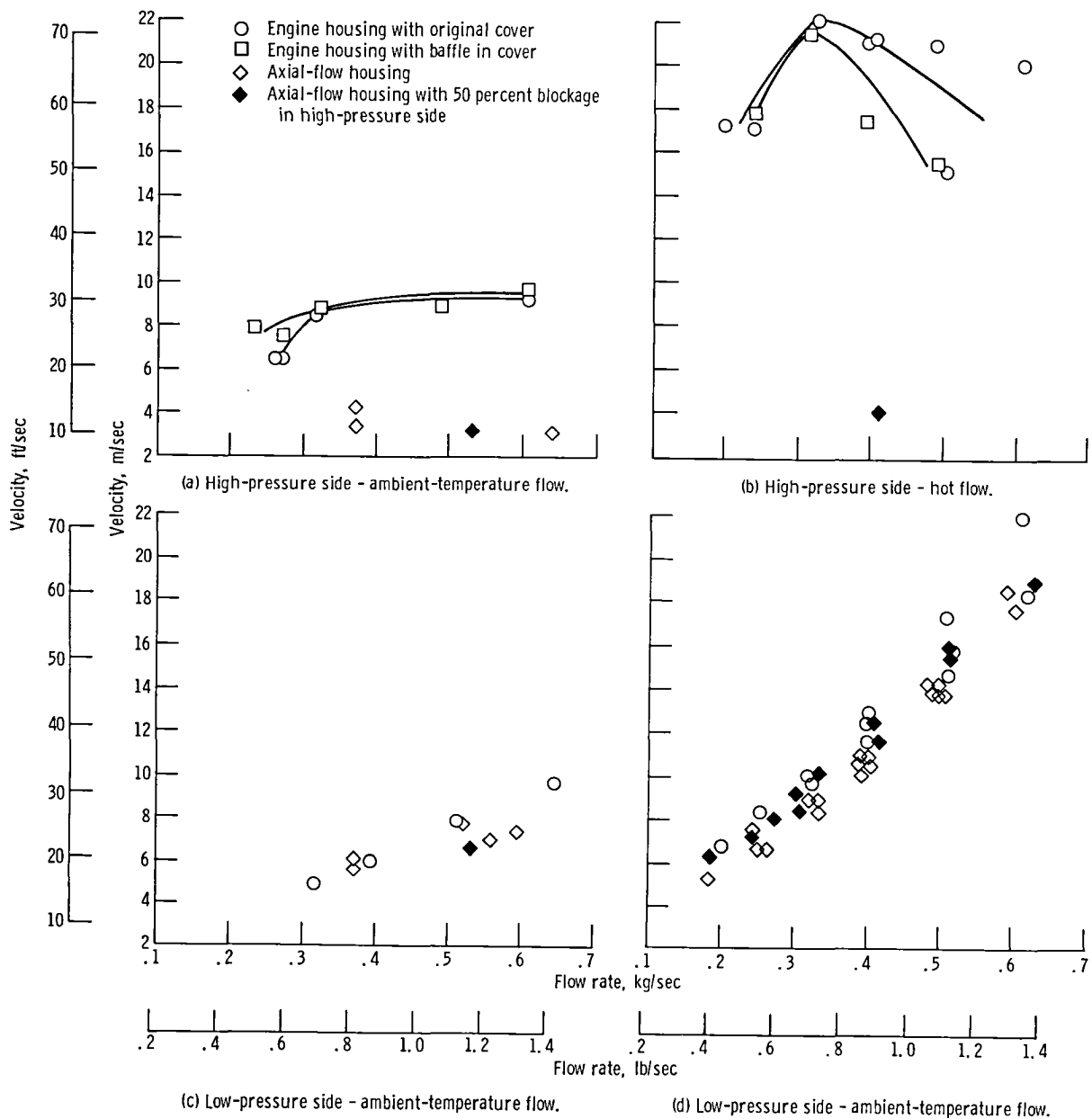
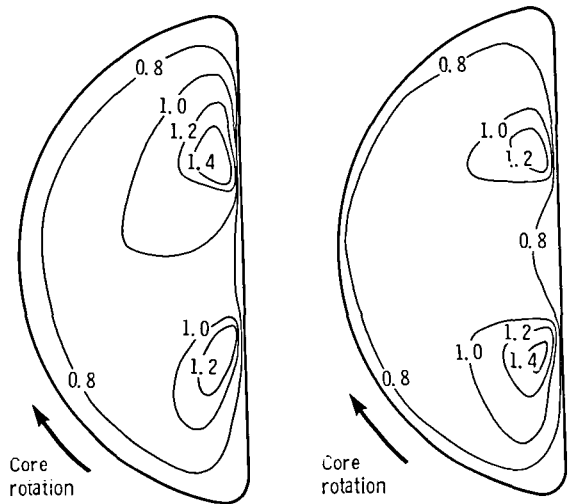


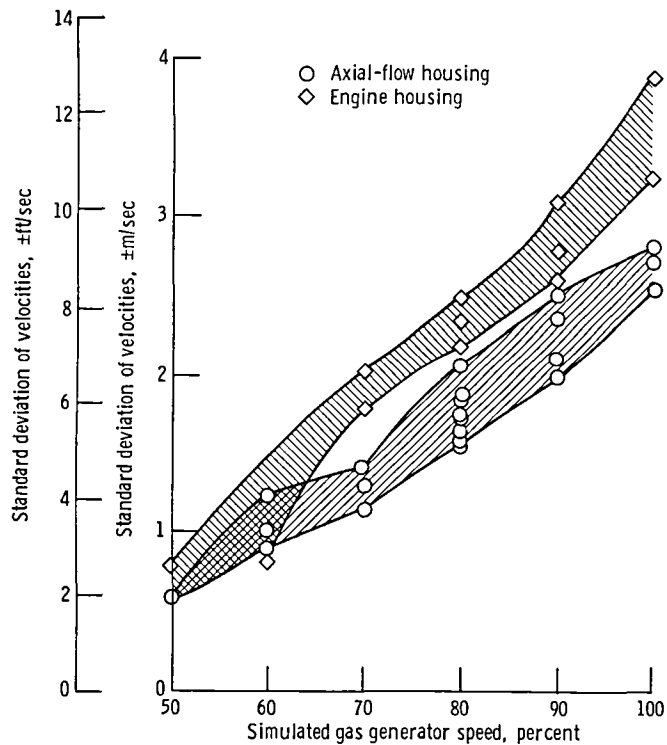
Figure 37. - Average velocities.



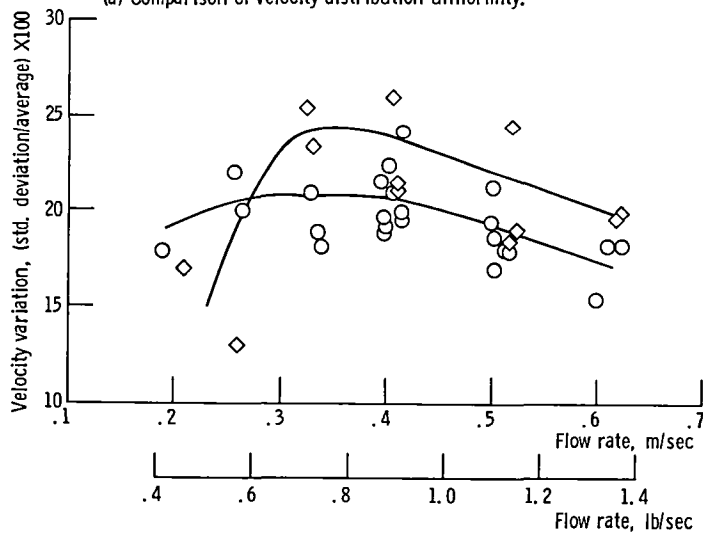
(a) 90 Percent of simulated gas generator speed.

(b) 100 Percent of simulated gas generator speed.

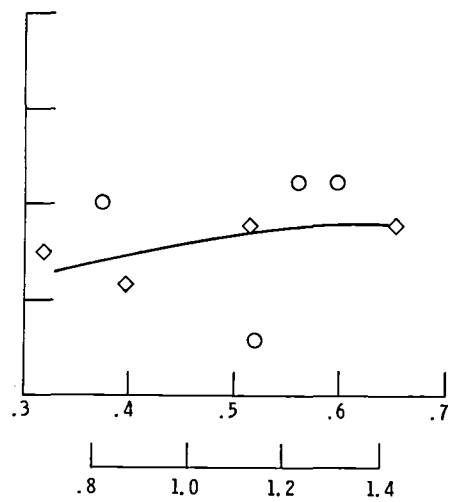
Figure 38. - Low-pressure-side velocity map - axial-flow housing; not flow.



(a) Comparison of velocity distribution uniformity.



(b) Velocity uniformity comparison - hot flow.



(c) Velocity uniformity comparison - ambient-temperature flow.

Figure 39. - Statistical measure of low-pressure-side velocity uniformity - engine and axial-flow housings.

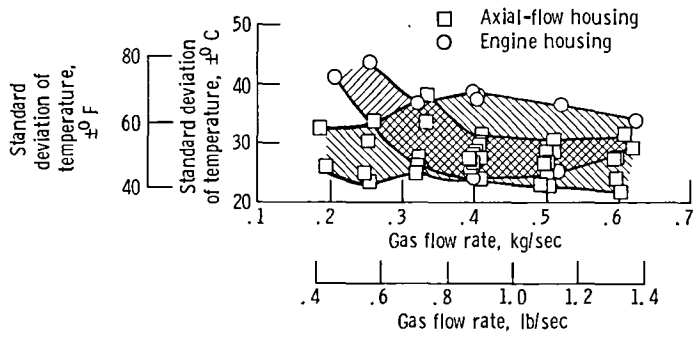


Figure 40. - Low-pressure-side temperature output uniformity - engine and axial-flow housings.

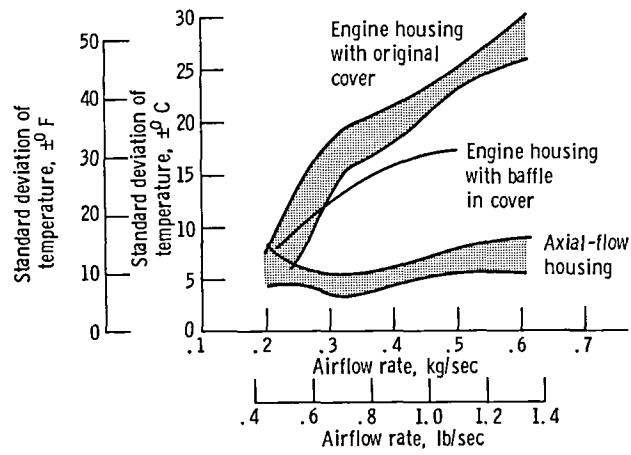
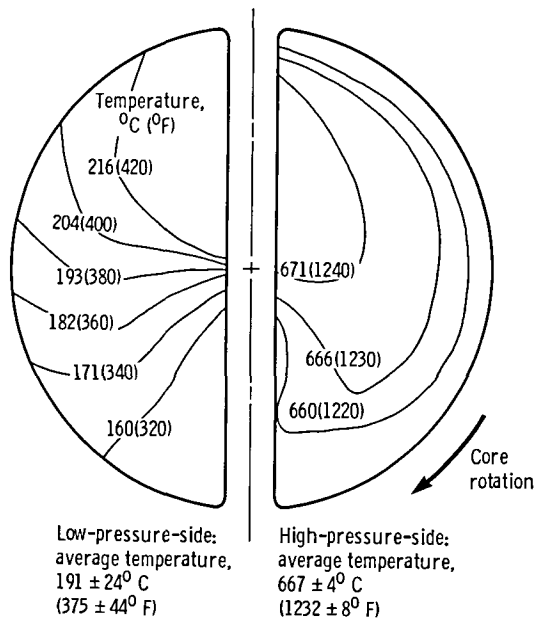
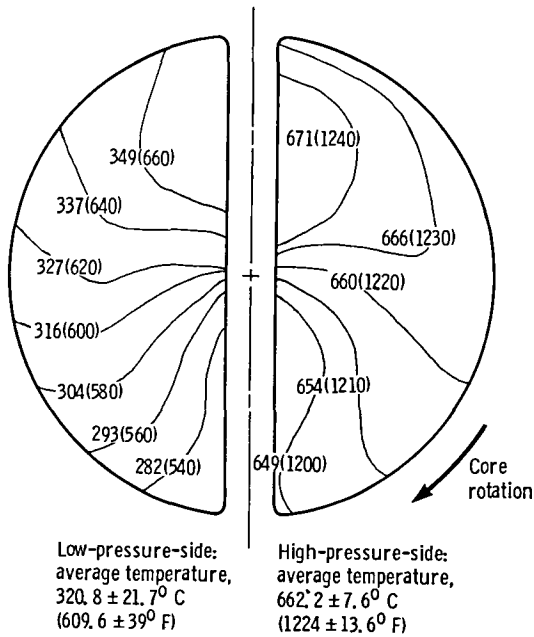


Figure 41. - High-pressure-side temperature output uniformity - original and modified engines and axial-flow housings.



(a) 60 Percent of simulated gas generator speed.



(b) 100 Percent of simulated gas generator speed.

Figure 42. - Temperature map - axial-flow housing.

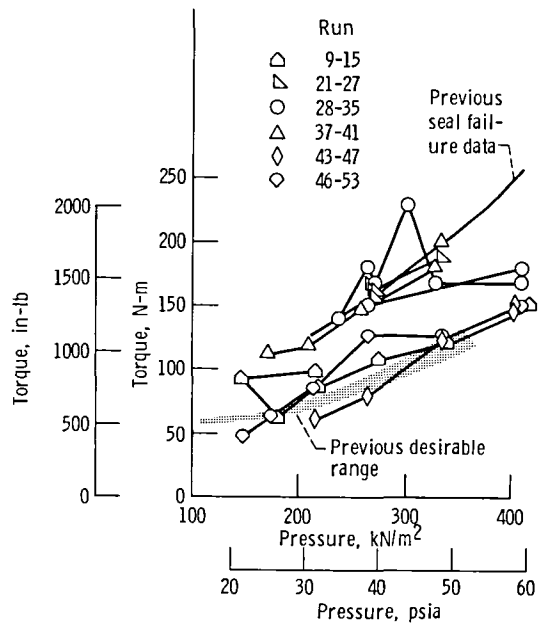


Figure 43. - Measured torque - axial-flow housing.

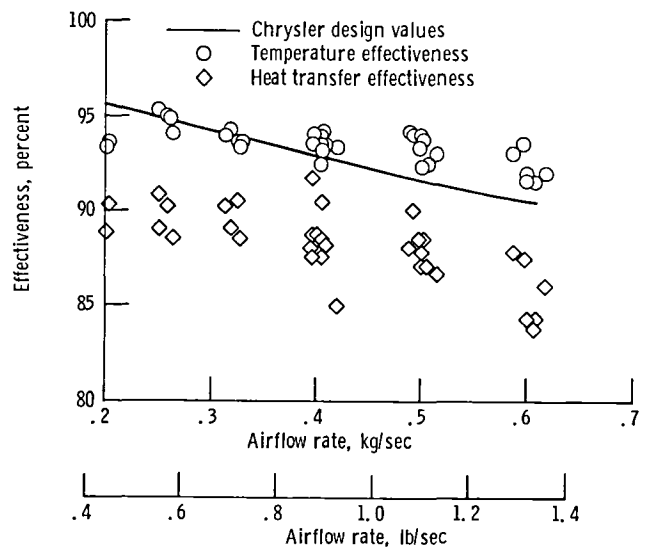


Figure 44. - Regenerator effectiveness - axial-flow housing.

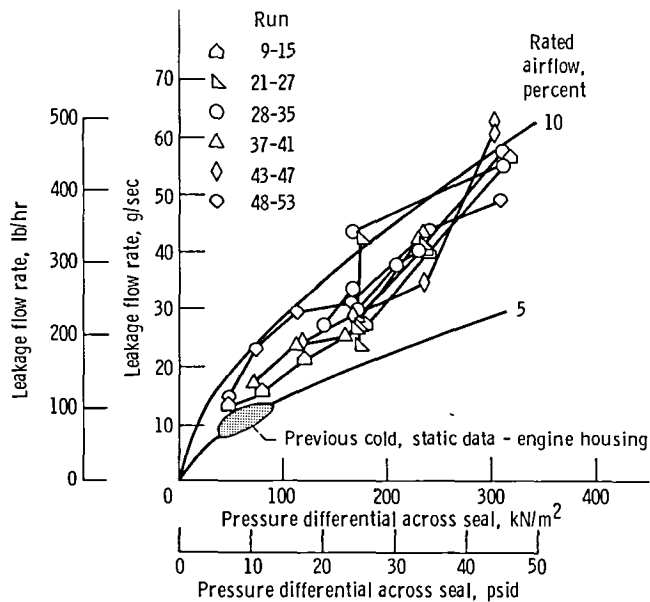


Figure 45. - Measured leakage - axial-flow housing.

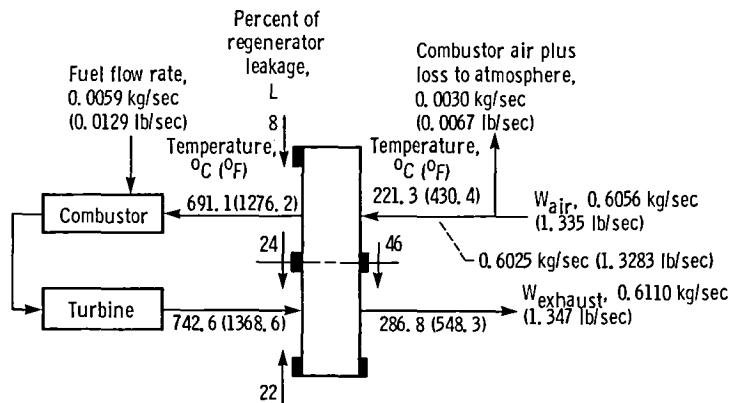


Figure 46. - Chrysler values for regenerator performance at 100-percent engine operating condition. Regenerator leakage $L = 1.8$ percent $W_{air} = 0.0112$ kg/sec (0.0246 lb/sec).

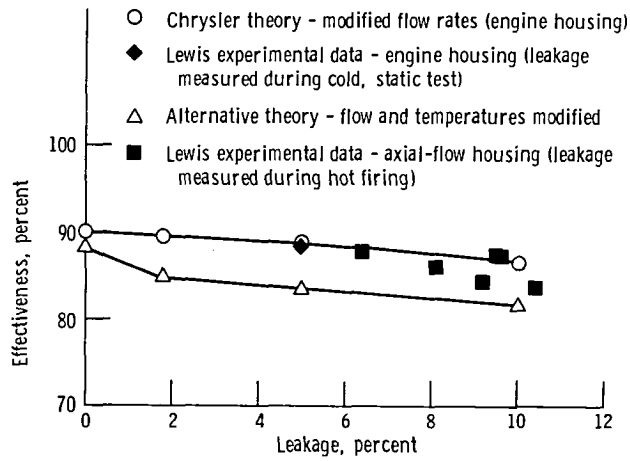


Figure 47. - Chrysler values for regenerator heat transfer effectiveness at 100 percent of gas generator speed.

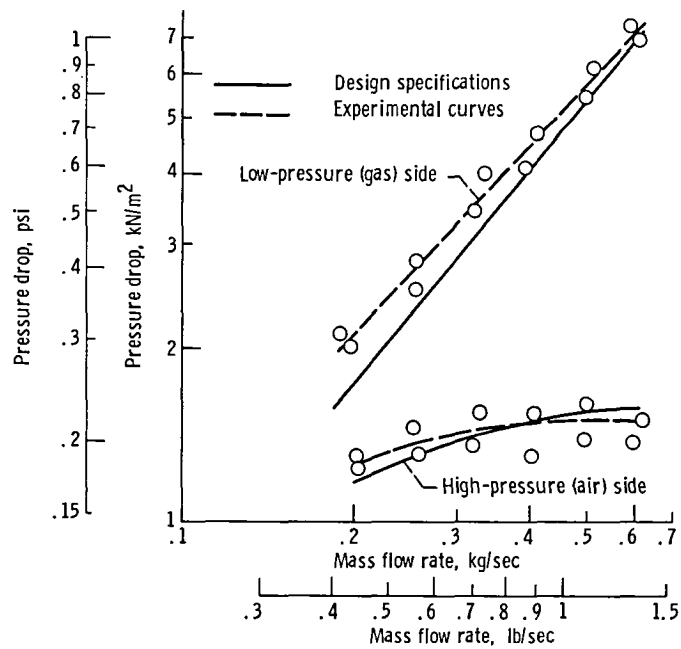


Figure 48. - Regenerator pressure drop - axial-flow housing.

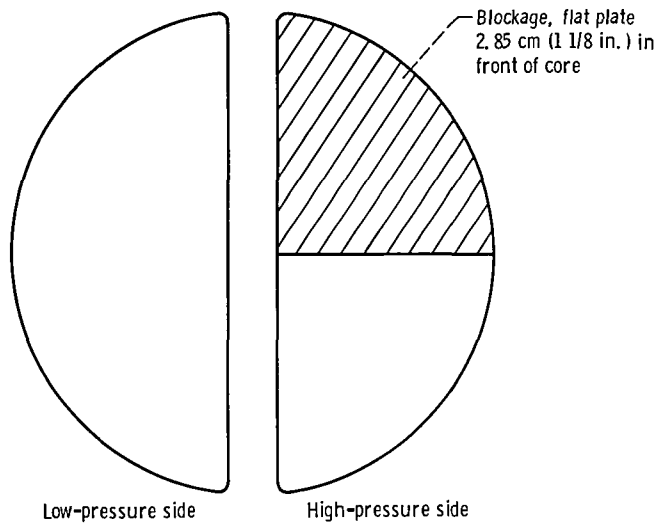


Figure 49. - Axial-flow-housing 50-percent-blockage configuration.

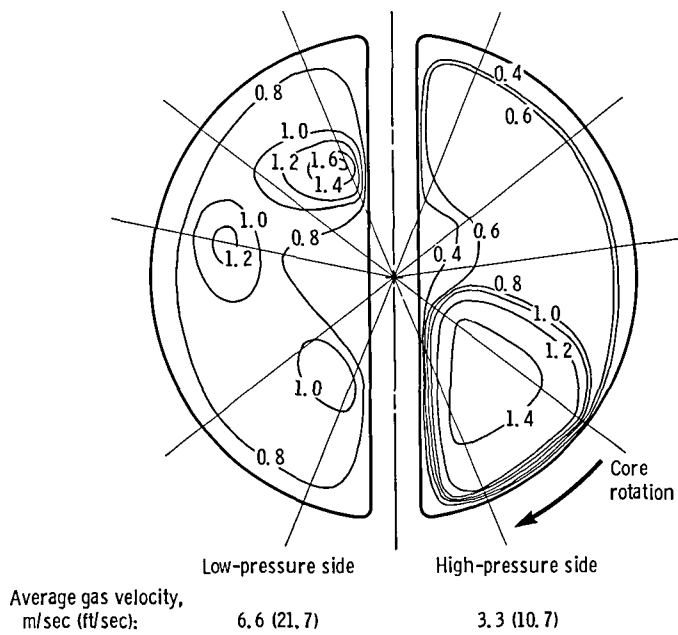
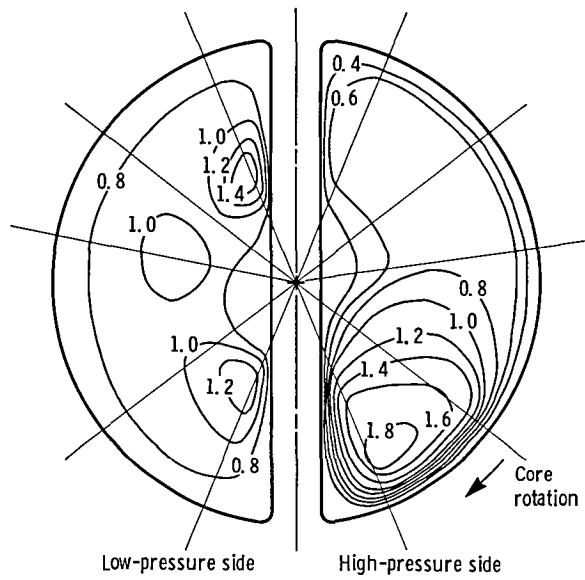


Figure 50. - Velocity map - axial-flow housing with 50 percent blockage in high-pressure inlet. Airflow rate, 0.53 kg/sec (1.17 lb/sec); ambient-temperature flow.



Average gas velocity,
 m/sec (ft/sec): 9.7 (31.8) 4.1 (13.5)

Figure 51. - Velocity map - axial-flow housing with 50 percent blockage upstream of high-pressure inlet. Simulates 80 percent of gas generator speed.

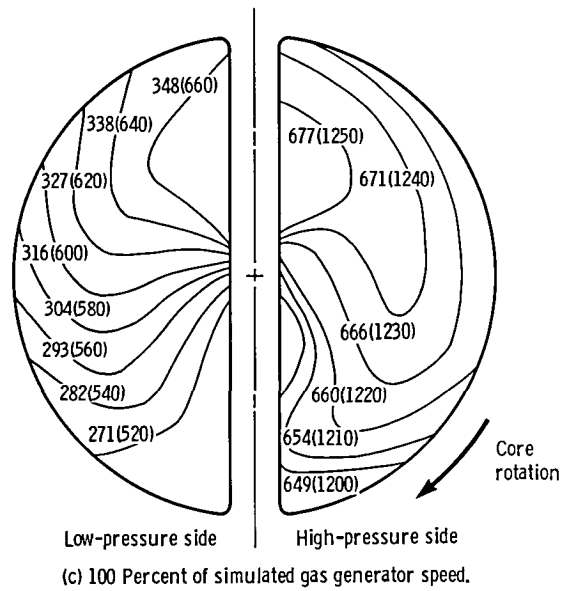
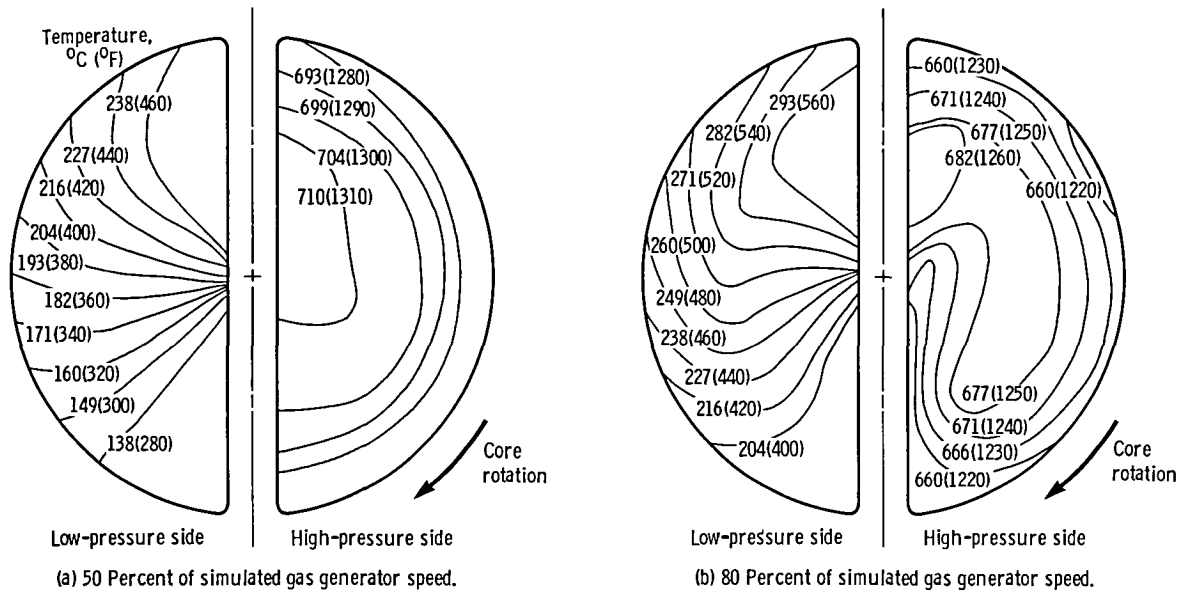


Figure 52. - Temperature map - axial-flow housing with 50 percent blockage in high-pressure inlet.

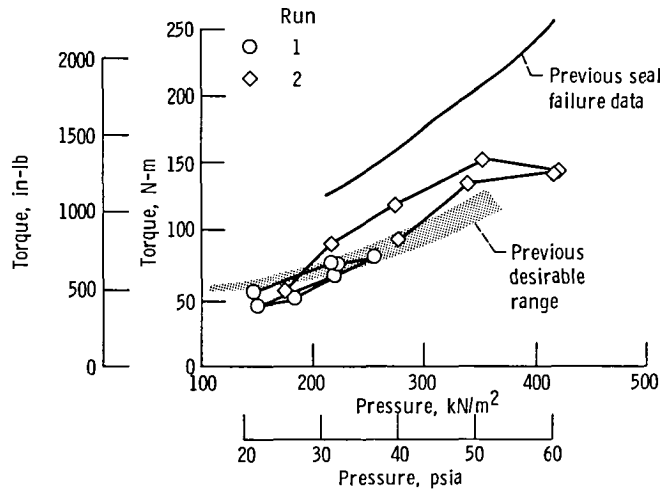


Figure 53. - Measured torque - axial-flow housing with 50 percent blockage in high-pressure inlet.

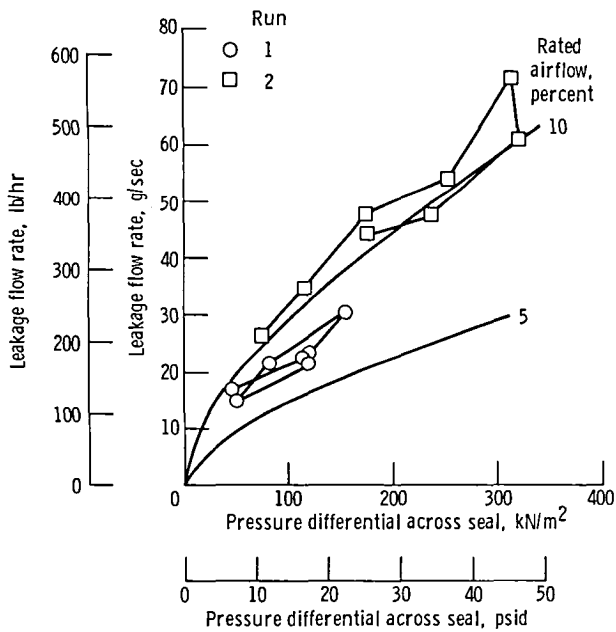


Figure 54. - Measured leakage during hot firing - axial-flow housing with 50 percent blockage in high-pressure inlet.

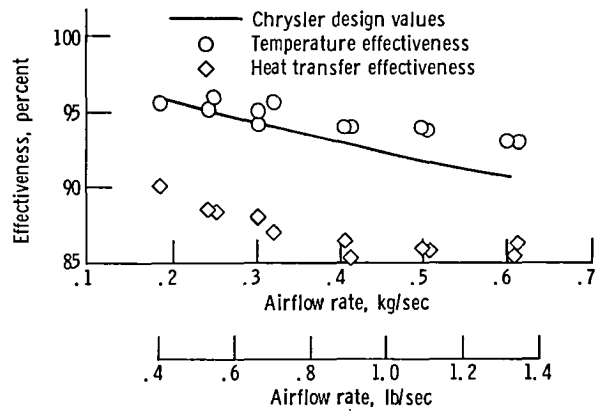


Figure 55. - Regenerator effectiveness - axial-flow housing with 50 percent blockage in high-pressure inlet.

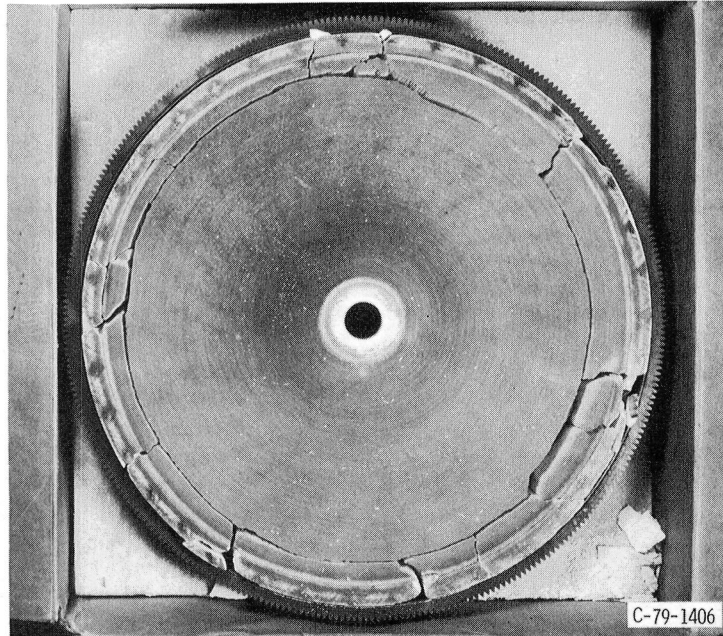


Figure 56. - Failed regenerator.

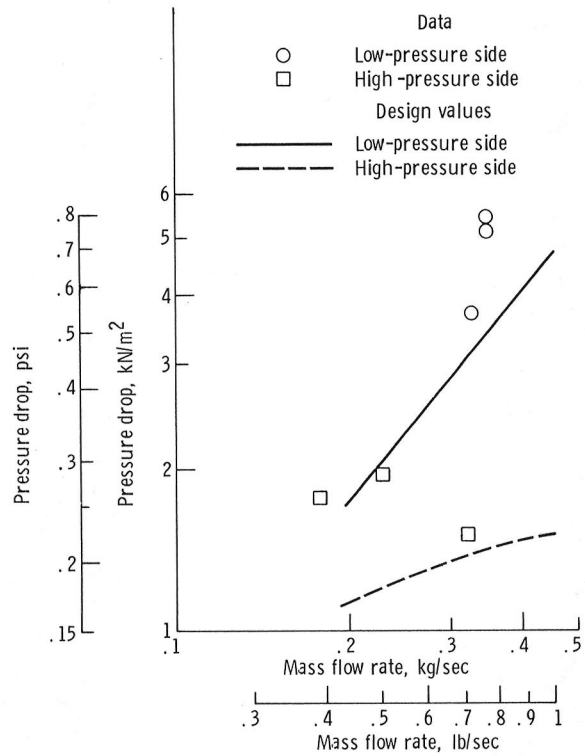


Figure 57. - Regenerator pressure drop during transient testing - axial-flow housing.

1. Report No. NASA TM-82671		2. Government Accession No.		3. Recipient's Catalog No.	
4. Title and Subtitle EXPERIMENTAL PERFORMANCE OF THE REGENERATOR FOR THE CHRYSLER UPGRADED AUTOMOTIVE GAS TURBINE ENGINE			5. Report Date February 1982		
			6. Performing Organization Code 778-32-01		
7. Author(s) Jerry M. Winter and Ralph C. Nussle			8. Performing Organization Report No. E-953		10. Work Unit No.
9. Performing Organization Name and Address National Aeronautics and Space Administration Lewis Research Center Cleveland, Ohio 44135			11. Contract or Grant No.		
			13. Type of Report and Period Covered Technical Memorandum		
12. Sponsoring Agency Name and Address U. S. Department of Energy Office of Vehicle and Engine R&D Washington, D. C. 20545			14. Sponsoring Agency Code Report No. DOE/NASA/51040-32		
			15. Supplementary Notes Final report. Prepared under Interagency Agreement DE-AI01-77CS51040.		
16. Abstract <p>Regenerator performance was studied in a regenerator test facility that provided a satisfactory simulation of the actual engine operating environment but with independent control of airflow and gas flow. Velocity and temperature distributions were measured immediately downstream of both the core high-pressure-side outlet and the core low-pressure-side outlet. For the original engine housing, the regenerator temperature effectiveness was 1 to 2 percent higher than the design value, and the heat transfer effectiveness was 2 to 4 percent lower than the design value over the range of test conditions simulating 50 to 100 percent of gas generator speed. Recalculating the design values to account for seal leakage decreased the design heat transfer effectiveness to values consistent with those measured herein. A baffle installed in the engine housing high-pressure-side inlet provided more uniform velocities out of the regenerator but did not improve the effectiveness. A housing designed to provide more uniform axial flow to the regenerator was also tested. Although temperature uniformity was improved, the effectiveness values were not improved. Neither did 50-percent flow blockage (90° segment) applied to the high-pressure-side inlet change the effectiveness significantly. Regenerator drive torque varied from 57 N-m (500 in-lb) at 50 percent of simulated gas generator speed to 171 N-m (1500 in-lb) at 100 percent speed. These torques correspond to 67 and 440 W (0.09 and 0.59 hp), respectively, at the regenerator design speeds. The measured leakage rates for these torques were 5 percent of the total airflow at 50 percent of simulated gas generator speed and up to 12 percent of the total airflow at 100 percent of simulated gas generator speed. The areas most in need of development were seal material and application techniques to decrease leakage while maintaining reasonable torque values.</p>					
17. Key Words (Suggested by Author(s)) Regenerator; Heat transfer; Automotive gas turbine			18. Distribution Statement Unclassified - unlimited STAR Category 44 DOE Category UC-96		
19. Security Classif. (of this report) Unclassified		20. Security Classif. (of this page) Unclassified		21. No. of Pages 62	22. Price* A04

* For sale by the National Technical Information Service, Springfield, Virginia 22161

National Aeronautics and
Space Administration

Washington, D.C.
20546

Official Business
Penalty for Private Use, \$300

THIRD-CLASS BULK RATE

Postage and Fees Paid
National Aeronautics and
Space Administration
NASA-451



NASA

POSTMASTER: If Undeliverable (Section 158
Postal Manual) Do Not Return
